catalysts

MDPI

Review

Factors Controlling the Redox Activity of Oxygen in Perovskites: From Theory to Application for Catalytic Reactions

Chunzhen Yang [1] and Alexis Grimaud [1,2,3,*]

[1] Chimie du Solide et de l'Energie, UMR 8260, Collège de France, 75231 Paris CEDEX 05, France; chunzhen.yang@college-de-france.fr

[2] Réseau sur le Stockage Electrochimique de l'Energie (RS2E), CNRS FR3459, 33 rue Saint Leu, 80039 Amiens CEDEX, France

[3] Sorbonne Université, UPMC, Paris 06, 75005 Paris, France

* Correspondence: alexis.grimaud@college-de-france.fr

Academic Editors: Yang Shao-Horn and Christian Jooss
Received: 25 January 2017; Accepted: 4 May 2017; Published: 11 May 2017

Abstract: Triggering the redox reaction of oxygens has become essential for the development of (electro) catalytic properties of transition metal oxides, especially for perovskite materials that have been envisaged for a variety of applications such as the oxygen evolution or reduction reactions (OER and ORR, respectively), CO or hydrocarbons oxidation, NO reduction and others. While the formation of ligand hole for perovskites is well-known for solid state physicists and/or chemists and has been widely studied for the understanding of important electronic properties such as superconductivity, insulator-metal transitions, magnetoresistance, ferroelectrics, redox properties etc., oxygen electrocatalysis in aqueous media at low temperature barely scratches the surface of the concept of oxygen ions oxidation. In this review, we briefly explain the electronic structure of perovskite materials and go through a few important parameters such as the ionization potential, Madelung potential, and charge transfer energy that govern the oxidation of oxygen ions. We then describe the surface reactivity that can be induced by the redox activity of the oxygen network and the formation of highly reactive surface oxygen species before describing their participation in catalytic reactions and providing mechanistic insights and strategies for designing new (electro) catalysts. Finally, we give a brief overview of the different techniques that can be employed to detect the formation of such transient oxygen species.

Keywords: oxygen redox activity; perovskite; charge transfer energy; electrocatalysts; oxygen evolution reaction (OER)

1. Introduction

Transition metal oxides have been the subject of numerous works owing to their singular electronic, magnetic, catalytic, and other properties that arise for most of them from the iono-covalent nature of the transition metal–oxygen bond [1]. Indeed, researchers initially assumed that metal *d* orbitals would provide an accurate description of the electrons in bands formed in the crystal, later it was suggested that an iono-covalent metal–oxygen bond must be taken into account to accurately describe the electronic structure of a transition metal oxide [2]. Hence, with discoveries in the last decades in the fields of high-T_c supraconducting materials, magnetic-exchange interactions but also in heterogeneous catalysis or electrocatalysis, a better description of the metal–oxygen bond became crucial in understanding the physical properties of transition metal oxides.

The perovskite AMO_3, whose structure can be simply described by the arrangement of MO_6 octahedra connected by corners and forming cages into which the A-site cation is in a twelve-fold

coordination, is the prototypical iono-covalent structure. Due to the unique flexibility of this family in accepting a large variety of cations in A- or M-sites, the electronic conductivity of perovskites can be tuned from insulating to metallic, with numerous magnetic properties being reported [3]. In addition to the traditional physical properties of perovskites, the importance of ligand hole formation, studied in depth during the supraconducting era following the discovery of high-T_c materials in 1986 [4], has recently being revisited since it can offer a unique opportunity to modify the catalytically active redox center on the surface of perovskites for the low temperature oxygen evolution reaction (OER), one half reaction of water splitting [5–7]. However, triggering and controlling the redox activity of oxygen on the surface of perovskite materials has been shown to be challenging, therefore requiring a deeper understanding of this phenomenon in order to develop new redox active compounds.

Before describing the electronic structure of perovskites and their electrocatalytic properties, the concept of oxidation of oxygen ions, sometimes defined as the oxygen redox reaction, needs some clarification, since it might be understood differently depending on the field of applications. Hence, while the high temperature gas phase catalysis community understand the term of "oxygen redox reaction" as the formation and the migration of oxygen vacancies, researchers from the field of low temperature electrocatalysis, or from the battery community, would refer this term to the involvement of the O^-/O^{2-} redox couple in an electrochemical reaction. The community of high temperature heterogeneous catalysis, in particular the field of solid oxide fuel cells (SOFC), is well aware of the possibilities given by formation of oxygen vacancies and surface oxygen exchange [8–12]. The physical properties of oxygen vacancies, such as their density, in crystal structure, enthalpy of formation, diffusion kinetics or else playing an important role in catalytic reactions, has been extensively studied and for which the use of high temperature provides the energy to drive their formation and diffusion [8–13]. We refer the readers to the above mentioned citations for further details on this topic which is not the main focus of this review.

Rather than their "defect chemistry", when using perovskites as catalysts for water splitting and other electrocatalytic reactions occurring at room temperature, we must first understand where electrons are taken from under oxidative conditions, i.e., which is the redox center participating in the reaction. Hence, the electronic density of state is the tool of choice when considering low temperature electrochemical reactions. However, more importantly, when considering reactions involving the formation of chemicals, the description of molecular orbitals becomes of prime importance since reactivity and bond formation/breaking are invoked. Indeed, while a redox center based on strongly covalent M–O bonds would allow for the insertion of adsorbed O^- species on the surface of perovskites used as SOFC electrodes at high temperatures [14,15], the reactivity of these species towards water largely differs from one of the $O^{\cdot -}$ (or oxyl groups) which are formed by removing electrons from *p* orbitals of oxygen that do not participate in the formation of an M–O bond (lone pair). In other words, removing an electron from a lone pair leads to the formation of an unpaired electron which is defined in chemistry as a radical species ($O^{\cdot -}$). Identifying the difference between these two types of oxidized species formed under oxidation is also of prime importance for storing extra capacity in Li-ion battery cathode materials, since only the electron removal from lone pair orbitals offers the opportunity to exchange an extra electron upon charging in addition to the one classically exchange from the M–O* bond. Hence, several papers can be found in the literature regarding this phenomenon, with a common agreement in describing the anionic (or oxygen) redox reaction as involving oxygen lone pairs [16–23]. Definitively, it now appears that the chemistry of O–O bond formation, which is the cornerstone of the OER reaction for instance, involves specific electronic levels that we aim to describe in this manuscript.

Additionally, the oxygen vacancy formation in the crystal structure has been shown to be correlated to the electronic structure of oxides. Nevertheless, a defect chemistry approach cannot be applied to study the redox behavior of perovskites as it only brings an indication about the charge balance at the final stage of the electrochemical process. Instead, when considering electrocatalytic reactions, importance is paid on the rate limiting step that controls the kinetics of the reaction and which is often associated with electron transfer between the catalyst and the adsorbate. Hence,

in this manuscript, we tentatively explain the electronic levels involved in the O^-/O^{2-} redox couple, as well as describing the reactivity of oxygen as reactive sites deciphered from a classical band structure approach.

Therefore, we aim to provide a simple description of the oxidation of oxygen ions in perovskite materials to readers in the field of water splitting and other low temperature electrocatalytic reactions, who might neither be familiar with this concept nor with the description of the electronic structure for transition metal oxides. Hence, rather than a full description of the electronic structure for various perovskites, we aim to shed light on some theoretical concepts and experimental techniques that would allow readers to understand the different mechanisms encountered when using perovskites as OER catalysts. Indeed, for the rational design of electrocatalysts with high activity and enhanced stability, it is important to combine theoretical and experimental approaches to achieve a level of consistency and complementarity in our understanding.

The first part of the manuscript is devoted to explaining step by step how the electronic structure of perovskite materials can be simply described. By doing so, the so-called cationic and anionic redox reactions are explained. Then, we go through some parameters that have an impact on accessing non-bonding oxygen states. We systematically describe the $LaM^{3+}O_3$ and $SrM^{4+}O_3$ series, with M being a series of 3*d* transition metals, so as to obtain qualitative trends that can be used to design new perovskites with redox active oxygen ions. In the second part, experimental reports for the oxidation of oxygen ions and their participation as active sites for electrocatalytic reactions are discussed. Through these examples, we aim to demonstrate the unique opportunities given by using surface oxygen as a catalytic center for electrocatalytic reactions, such as the OER, when compared to metallic centers. We will not hide our understanding that the involvement of oxygen as a redox active site for the OER reaction is still at its infant state and that limitations remain, in particular in terms of surface stability, therefore calling for further studies to fully explore this phenomenon. Finally, we discuss experimental techniques that allow oxygen to be spotted as an active redox center in perovskites.

2. Perovskites' Electronic Structure

Before any description of the role of oxygen as an active site for the OER, general ideas on the electronic structure of perovskite oxides must be given. In a crystal structure, cations are surrounded by negatively charged oxygen which creates a repulsive effect to the electrons of cations, eventually destabilizing their energy. This repulsive term, known as the Madelung potential, is dependent on the crystallography and is obtained by summing the electrostatic interactions q^2/r, with q being the charge and r being the interatomic distance. In an opposing manner, the energy of oxygen anions is stabilized by the surrounding positively charged cations, lowering the energy of the oxygen orbitals in the crystal (Figure 1). In the perovskite crystal structure, transition metals are in an octahedral environment in which d_{z^2} and $d_{x^2-y^2}$ atomic orbitals have strong spatial overlap with the oxygen *p* orbitals pointing towards them, forming σ bonding MO and antibonding MO* molecular orbitals destabilized in energy and called e_g (note that not every orbital is represented in Figure 1). The metallic orbitals with no direct overlap with the oxygen orbitals form π bonding MO and antibonding MO* states which are less destabilized in energy than the e_g and referred to as t_{2g} states. These MO and MO* states have a degree of metallic and oxygen character which is given by the difference in electronegativity of the cationic and oxygen states, i.e., by the covalence of the M–O bond. However, the oxygen character never exceeds that of the metal for the antibonding states. Therefore, these states are often referred to as cationic *d* states (Figure 1, right panel). With three oxygens (having each three 2*p* orbitals) per metal (having five *d* orbitals) in the perovskite AMO_3, some oxygen orbitals may not hybridize with metallic states, depending on the symmetry of the structure, hence forming non-bonding and purely oxygen *p* states. These states are referred to as ligand states, in contrast to MO* states that remains mostly cationic in character. When using perovskites under oxidative conditions, i.e., applying a positive potential, two types of redox centers can therefore be attained: the first one involving the electron removal from an MO* state and described as a cationic redox reaction since its oxygen "character" never exceeds

50%, and the second one for which electrons are taken from non-bonding oxygen states and denoted as an oxygen redox reaction. Even though oxygen ions can be partially oxidized by removing an electron from the MO* states in a strongly covalent structure, the so-called ligand hole formed through this process is delocalized contrary to the holes created in purely oxygen states, making their reactivity towards water or other molecules very different. Throughout this manuscript, we will describe the oxygen species formed on the surface of perovskites by electron removal from purely oxygen states as oxyl groups.

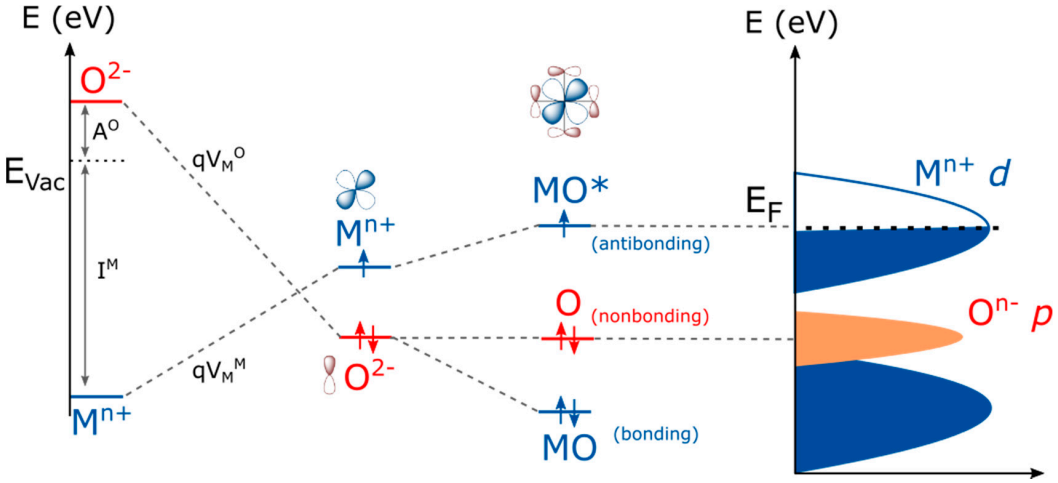

Figure 1. Formation of a density of states for perovksites with the different contributions, starting from the ionization energy of metals (I^M) as well as the electron affinity of the oxygen (A°), the Madelung site potentials (V_M^M with V_M^O for the metal and the oxygen, respectively) corresponding to the reticulation energy shifting the energy of ions in a crystal structure, the crystal field interaction forming antibonding MO* (usually called *d* band), purely oxygen non-bonding O states (described as *p* states) and bonding MO orbitals from the atomic M and O orbitals which finally form in an extended 3D crystal bands that can be integrated to obtain a so-called density of state diagram, representing the electronic density for each state as a function of the energy. Note that for AMO_3 perovskites, 5*d* orbitals from the transition metals and 3×3 *p* orbitals from oxygen are involved. Hence, this representation does not show every electron and orbital involved in the electronic structure of perovskites.

3. Use of Simple Pictures to Predict the Formation of Holes in Purely Oxygen States

When using perovskites as catalysts for electrochemical oxidation processes, the electronic structure might predict when a so-called "oxygen redox reaction" will be triggered, instead of a classical cationic one. First, a simplified picture for which M–O bonds are considered as purely ionic will be used so to estimate the energy required to remove an electron from an oxygen state. Then, the limitations inherent in the use of an ionic model will be discussed, before providing a more accurate covalent model. We will show that even if imperfect, this model can capture relatively well the switch from a cationic to an anionic redox center for perovskite materials.

Following a simple ionic picture, the energy required to form a hole on a metallic site is given by the ionization energy of the metal (I_4^M the fourth ionization energy when considering $LaM^{3+}O_3$ perovskites for instance) plus eV_M^M, with V_M^M (in V) being the Madelung site potential of the metal. Similarly, the energy required to form hole on oxygen states is given by the second electron affinity of oxygen A_2^O plus eV_M^O, with V_M^O (in V) being the Madelung site potential of the oxygen. Therefore, the energy difference between a hole on the oxygen and on the metal is given by [24]:

$$\Delta E_h = A_2^O - I_4^M + e\left(V_M^O - V_M^M\right) \quad (1)$$

From this expression, two major contributions for the energy of formation of holes in transition metal oxides can be seen: one arising from the electronegativity of the metal itself (ionization energy) and the second one related to the electrostatic potential which is dependent on the structure itself. The calculated ΔE_h values as a function of *d* electrons for two series of perovskites $LaM^{3+}O_3$ and $AM^{4+}O_2$ (A being Sr^{2+} or Ca^{2+}) are reported in Figure 2a (energies are scaled vs. the energy calculated for $SrTiO_3$ which has been arbitrarily defined as 0 eV). From this simple calculation, it appears that d° oxides such as $SrTiO_3$ will preferably form holes on oxygen states when compared to other compounds. Indeed, one can easily understand that no holes can be formed in the mostly metallic MO* states which are empty and which lie well above the pure oxygen states for d° oxides. Hence, when oxidizing $SrTiO_3$, holes are formed in the oxygen states to form oxyl groups on the surface [25], as very recently spotted by ultrafast vibrational spectroscopy [26,27], before being eventually stabilized by forming O–O bonds on the surface [26]. Then, a clear trend can be observed for both the $LaM^{3+}O_3$ and $SrM^{4+}O_3$ series by moving from early to late transition metals (increasing the amount of *d* electrons), where the energy associated with the formation of a hole in the metallic states increases, following the ionization energy of the metal, and therefore the energy difference between the formation of a hole on the oxygen states and the metallic states decreases. Moreover, the limitations related to such a simple calculation based on a purely ionic picture can be seen in Figure 2a, where the formation of a hole on the oxygen states would appear less favorable energetically when oxidizing the metal from M^{3+} to M^{4+}. However, as largely accepted and reported, when increasing the oxidation state of the metal, its electronegativity increases and therefore the MO* bond decreases in energy to eventually enter into the purely oxygen states. Indeed, one can track the effect of the electronegativity of the metal on the position of the Fermi level by using the simple approach developed by Campet et al. [28], and for which the Fermi level, defined as the middle of the band gap, for a given metal at a given oxidation state follows the simple empirical linear relationship:

$$E_F = (-0.2z + 1.2603)X_M^{z+} + 1.13z - 0.17 \quad (2)$$

with *z* being the oxidation state and X_M^{z+} being the electronegativity of the corresponding metal ion, as reported by Matar et al. [29]. When applying this equation to M^{3+} and M^{4+} 3*d* transition metal oxides (Figure 3), one can easily observe the Fermi level going down in energy (i.e., its absolute energy vs. vacuum increasing) with the metal electronegativity as well as when oxidizing the transition metal from M^{3+} to M^{4+}. However, a more precise calculation of the electronegativity of the transition metal for the iono-covalent structure can be made by taking into account the "effective" charge of the metal and the oxygen. This method, initially developed for molecules [30] and later used for solid state compounds [31], was recently proven to be able to predict the redox potential for Lithium-ion battery materials [32].

When considering cubic or pseudocubic perovskites for which the M-O bond distance remains almost constant for 3*d* metals (from ≈1.95 Å for $SrTiO_3$ to ≈1.92 Å for $SrCoO_3$, for instance), no drastic modification of the Madelung potentials is seen along the series (Figure 2b). Therefore, in the perovskite structure for which the electrostatic interactions are largely governed by the large and polarizable A-site cation, the Madelung potential would remain constant for a given rare earth or lanthanide.

Using the Zaanen, Sawatzky and Allen (ZSA) framework for the Mott-Hubbard vs. Charge–Transfer insulators [33], the electronic band structure of transition metal oxides can be inferred from the relative value of the charge transfer Δ (energy between the occupied oxygen states and the unoccupied metallic states, i.e., the electronegativity difference between cation and anion) and the on-site Coulomb repulsion *U* corresponding to the energy between the unoccupied and the occupied metallic states (Figure 4a). Even though this model fails in fully capturing the physics of the highly correlated electron system, it was successfully applied to capture the redox activity for Li-ion batteries [16]. A way to estimate the covalent character of the M–O bond is given by the relative hybridization factor β which can approximate to T_{pd}/Δ (T_{pd} being the transfer integral). Knowing

that the transfer integral remains almost constant for perovskites along one row [34–36], the covalence of the M–O bond is therefore mainly governed by the charge transfer Δ [37].

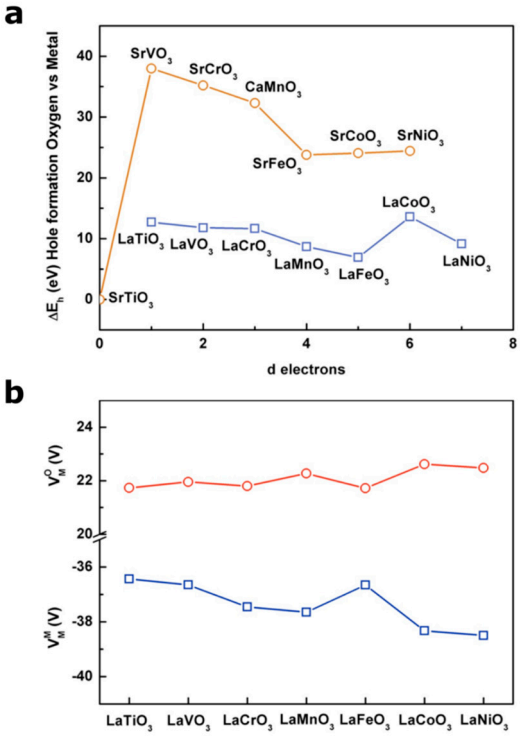

Figure 2. (**a**) Variation of the energy of hole formation on oxygen vs. hole formation on metal calculated from Equation (1) as a function of *d* electrons for cubic or pseudocubic $LaM^{3+}O_3$ (blue) and $AM^{4+}O_3$ (brown) perovskites. Note that 0 eV is arbitrarily given to $SrTiO_3$ (d°) as a reference. Madelung constants were obtained from Vesta software using reported structures, and the Madelung potentials were calculated from the method describe elsewhere [24]. The ionization energies were obtained from elsewhere [33]. $CaMnO_3$ was chosen due to its pseudocubic symmetry rather than $SrMnO_3$ which possesses hexagonal structure. Note that no Ni^{4+} containing perovskite shows a pseudocubic lattice and $SrNiO_3$ used in this plot shows the hexagonal 2H structure. (**b**) Oxygen Madelung potentials (V_M^O) and metal Madelung potentials (V_M^M) calculated for the $LaM^{3+}O_3$ series using a classical approach.

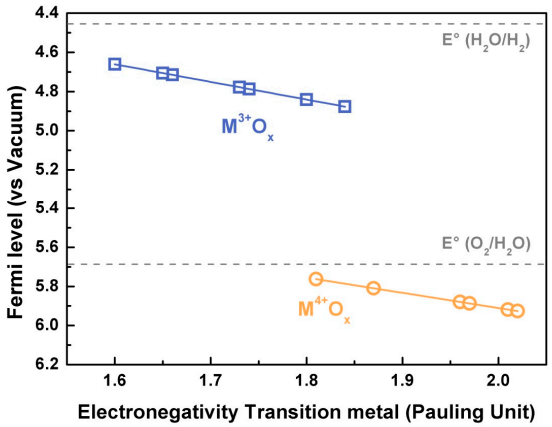

Figure 3. Fermi level calculated for M^{3+} and M^{4+} 3*d* metal following the simple equation developed by Campet et al. [28] as a function of the transition metal electronegativity (in Pauling unit) as calculated by Matar et al. [29]. The Fermi levels calculated with equation (2) correspond to the middle of the band gap, and are compared to the standard potential H_2O/H_2 and O_2/H_2O at pH = 0.

A so-called Mott-Hubbard regime is expected when $U < \Delta$, with the occupied MO* cationic states lying below the Fermi level (Figure 4a). In this case, the ground state is simply $|d^n\rangle$ and upon oxidation the redox reaction is expected to be cationic. When a charge-transfer regime is found ($U > \Delta$) (Figure 4c), the pure non-bonding O *p* states may lie at the Fermi level, depending on the symmetry of the M-O bonds, and the ground state configuration would be either $|d^n\rangle$ for an ionic M-O bond or a mixture $|d^n\rangle + |d^{n-1}\underline{L}\rangle$ when increasing the covalence of the metal-oxygen bond ($\underline{L}$ denotes a ligand hole). However, when $\Delta < 0$ (negative charge transfer material), the Fermi level enters into the O *p* states to form a purely $|d^{n-1}\underline{L}\rangle$ ground state. In any case, when $U > \Delta$, as the Fermi level is pinned to the oxygen states, the redox activity of oxygen states can be expected upon oxidation.

The effective charge transfer Δ_{eff} values found in the literature for the $LaM^{3+}O_3$ and $AM^{4+}O_3$ series are reported in Figure 4d (Δ_{eff} corresponds to the distance between the top of the *p* states and the bottom of the empty *d* states, while Δ corresponds to the distance between the middle of both bands). One can observe, not surprisingly, that going from M^{3+} to M^{4+} decreases the charge transfer gap, and therefore decreases the energy required to remove electrons from oxygen states. Hence, the charge transfer gap becomes zero for compounds such as $SrFeO_3$ [38] and even negative for $SrCoO_3$ [39,40], a so-called negative charge transfer material. As mentioned earlier, for these materials the oxygen is expected to be redox active. In addition to Fe^{4+}- and Co^{4+}-based perovskites, Ni^{3+}-based perovskites such as $NdNiO_3$ thin films have been recently discussed as possible negative charge transfer materials in order to explain their metal to insulator transition (MIT) [41]. Only few perovskites have been reported to be negative charge transfer materials, and, in addition to the aforementioned cobaltite or nickelate thin films [42], compounds such as $CaFeO_3$ or the A-site ordered $LaMn_3Cr_4O_{12}$ quadrupole perovskites were found to be negative charge transfer [43,44].

Interestingly, an intermediate case exists when $\Delta = U/2$, i.e., when both the MO* and the O *p* states lie at the Fermi level, and for which the redox reaction can be described as a mixture of anionic and cationic redox reaction (Figure 4b). In this case, the electron removal upon oxidation would imply that the Fermi level entered into a degenerated state for which MO* and O *p* states participate in the oxidation. Such a case is obviously unstable and charge reorganization is expected by reversing electrons from one band to the other, inducing the modification of the local structure through bond reorganization.

As discussed in the introduction, when removing electrons from oxygen states, oxygen vacancy can eventually be formed to keep the charge neutrality. Hence, one direct way to visualize the effect of the charge transfer energy on the oxidation of the oxygen ions network of perovskite compounds is given by plotting the calculated enthalpy of formation of oxygen vacancy for cobalt-based perovskites for instance as a function of the relative position of the oxygen states vs. the Fermi level, as recently studied by Lee et al. (Figure 4e) [8,9]. Not surprisingly, the energy required to form oxygen vacancies following the equation $O_O^x + 2h^{\cdot} \rightarrow V_O + 1/2O_{2(g)}$ decreases when lowering the energy between the oxygen states and the Fermi level, as previously described for the $La_{1-x}Sr_xCoO_{3-\delta}$ family [45]. For this, the electronegativity of the transition metal must be increased by using either high oxidation states or late transition metals, as discussed in Figure 3 and calculated by Maier and coworkers for different families of perovskites [12,46,47]. Furthermore, switching from 3*d* to 4*d* and 5*d* metals, the orbitals will become spatially more extended, increasing the covalence of the M-O bond but also decreasing the on-site Coulomb interaction *U*. Moreover, the use of 4*d* and 5*d* metals would also increase the charge transfer energy, as recently computed for layered Li_2MO_3 compounds [17] and experimentally verified for $SrMO_3$ perovskites [48], and therefore increase the energy required to oxidize oxygen states. A shift from charge transfer to a Mott-Hubbard regime is therefore expected. While oxygen states might be accessed by 3*d* when reaching an oxidation state close to M^{4+}, higher oxidation states would be required for 4*d* and 5*d* transition metals in order to access these states.

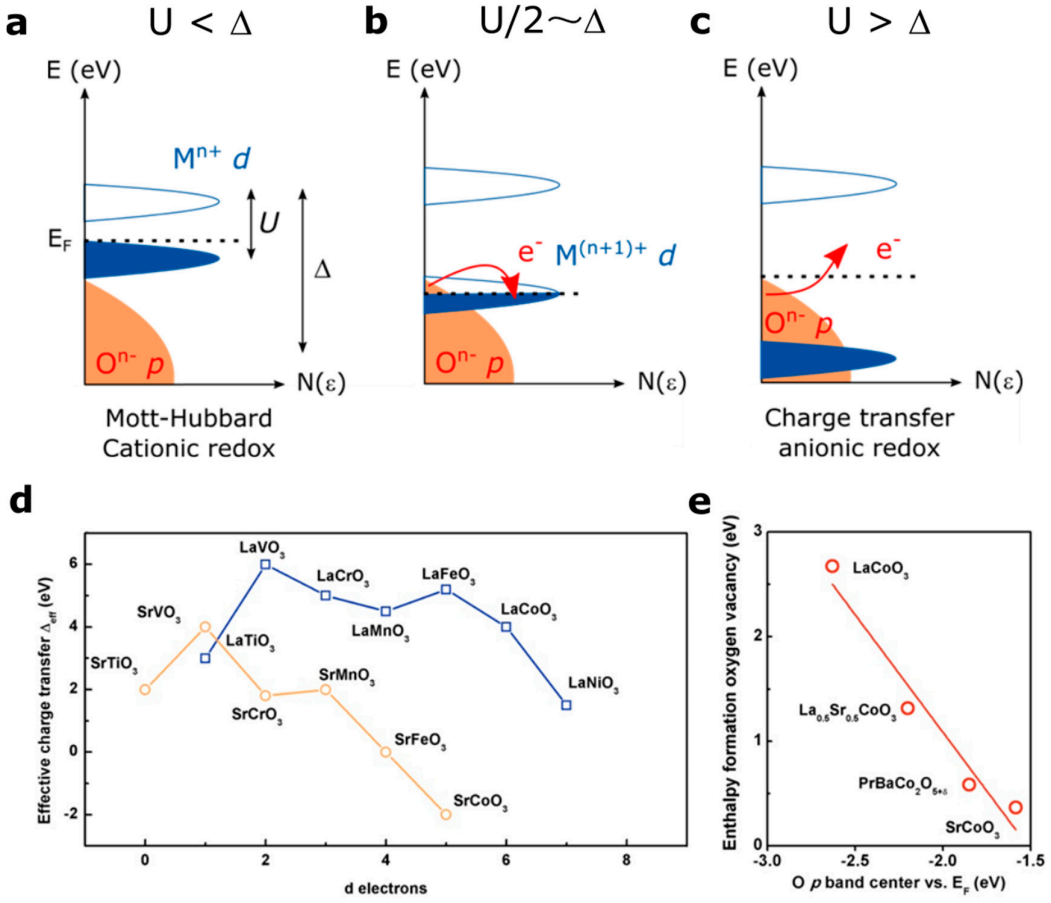

Figure 4. Zaanen-Sawatzki-Allen framework description of the electronic structure of transition metal oxides [33], with Δ the charge transfer gap and U the Coulomb inter-site repulsion with the case of (**a**) Mott-Hubbard regime (U < Δ) leading to a cationic redox reaction, (**b**) the intermediate case for which U/2 = Δ and (**c**) charge transfer regime (U > Δ) leading to an irreversible anionic redox reaction. (**d**) effective charge transfer values extracted from the literature for the $LaM^{3+}O_3$ and $SrM^{4+}O_3$ series [6,9,36,38,39] as well as (**e**) enthalpy of formation of an oxygen vacancy in cobalt-based perovskites as a function of the O *p* band energy vs. Fermi level, as reported in the literature [9].

Finally, bearing in mind that non-bonding oxygen *p* states are formed by oxygen *p* orbitals non-interacting with metallic *d* orbitals, one could simply look to increase the amount of oxygen *p* states in the perovskite density of states. One way to do so and eventually to trigger the anionic redox processes would be to decrease the metal/oxygen ratio within the perovskite structure, for instance forming Ruddlesden-Popper A_2MO_4 compounds. Taking the example of Li-ion or Na-ion batteries materials for which switching from layered transition metal oxides $LiMO_2$ to Li-rich layered compounds Li_2MO_3 was crucial to access the redox chemistry of oxygen upon charge [17,22,49–52], transition metal can be partially replaced by alkaline metal in the cubic perovskites in order to form La_2LiMO_6 compounds, for instance [23]. In addition to enabling the formation of non-bonding O *p* states, this strategy also offers a unique opportunity to stabilize the M–O bond with a greater covalence owing to the stabilization of the transition metal with a high formal oxidation state (5+ for the La_2LiMO_6 compounds). This situation would be largely favorable to form perovskites with oxygen ions as a redox center for electrocatalytic reactions.

4. Tuning the Perovskite Electronic Structure

At this stage, a legitimate question comes to mind: how can we further activate the redox activity of oxygen ions for perovskites if we are limited to only few oxidation states and transition

metals in order to increase the electronegativity of the metal? Even though the perovskite family is, strictly speaking, limited to AMO_3 compounds (if we neglect at that point Ruddelsden-Popper, Brownmillerite or other derivatives of the perovskite structure), modification of the A-site cation that shows no redox activity offers another degree of freedom in order to modulate the M–O bond and the electronic structure. Indeed, when modifying the ionic radius of the A-site cations, the so-called Goldschmidt tolerance factor t given by the ratio $\frac{r_A+r_O}{\sqrt{2}(r_M+r_O)}$ (with r_A the ionic radius of the A-site cation, r_O the ionic radius of the oxygen, and r_M the ionic radius of the transition metal) can be greatly modified (Figure 5a). When this factor, which indicates the stability and the distortion of the structure of the perovskite, exceeds the value of 1, the structure of the perovskite is no longer cubic and a so-called hexagonal perovskite is stabilized. Doing so, octahedra no longer share corners but faces, modifying the M–O bond distances as well as making possible interactions between transition metals. Therefore, through the strong distortion of the crystal field which is easily captured when comparing the Madelung potential of the metal (cobalt for instance) which increases at a given oxidation state from corner-($SrCoO_3$) to edge-(fully delithiated Li_0CoO_2) and face-shared ($BaCoO_3$) compounds (Figure 5b) as well as increases with the M–O bond distance, it can be deduced that hexagonal perovskites possess more covalent M–O bonds (lower absolute value for the Madelung potential for cobalt) when compared to cubic perovskites. This is visible by X-ray absorption measurements at the O K-edge, for which the pre-edge corresponding to the transition from O 1*s* to O 2*p*/M 3*d* hybridized state shows greater absorption for hexagonal perovskites than for cubic perovskites [53], presumably arising from a greater transfer integral T_{pd} owing to the shorter M–O bond distance. The hybridization of metallic and oxygen states and the existence of purely oxygen states largely depend on the local symmetry and, therefore, modifying the crystal field within the perovskite structure is expected to have a significant impact on creating and accessing purely oxygen states upon oxidation. This is particularly true when stabilizing trigonal prismatic symmetry in hexagonal perovskites for which the crystal field would lower the energy of the *d* orbitals (Figure 5c) [54].

Finally, the modulation of the electronic structure within the perovskite structure is perfectly exemplified by the $RNiO_3$ (R being a rare earth) family which has been extensively studied for its metal insulator transition. Within this family, the ionic radius of the A-site cation (from 1.36 Å for La^{3+} to 1.24 Å for Sm^{3+} in twelve-fold coordination for instance) [55,56] controls the O-M-O bond angle which eventually changes the conductivity behavior from insulating to metallic. While changing the A-site cation was shown to modify the transfer integral T_{pd}, the charge transfer gap Δ remains mostly constant for the different rare earth cations [37]. More importantly, the modification of the conducting behavior was shown to correlate to an increase of the metallic and oxygen band width (W_M and W_O, respectively) which closes the gap when using large rare earth cations (Figure 5d), making perovskites such as $LaNiO_3$ metallic while $SmNiO_3$ is insulating at low temperature [3,41]. Widening the bandwidth (increasing W) might therefore be an interesting strategy as it eventually lowers the effective charge transfer Δ_{eff} (defined as $\Delta - W$) and makes the oxygen *p* states easier to access upon oxidation.

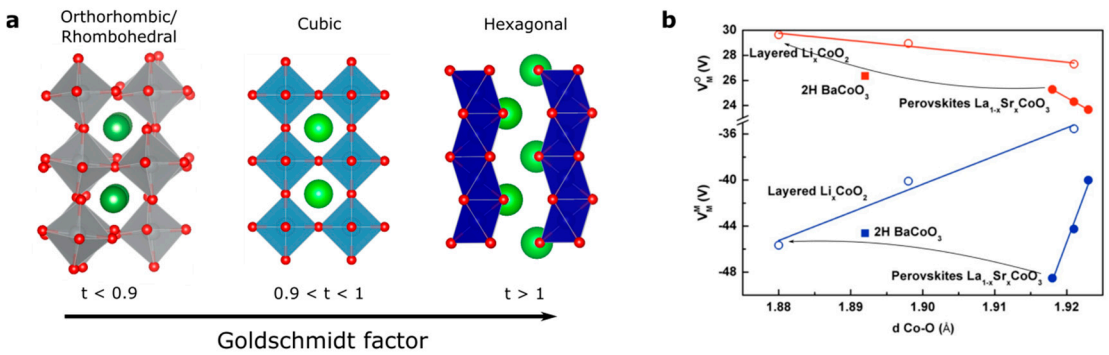

Figure 5. *Cont.*

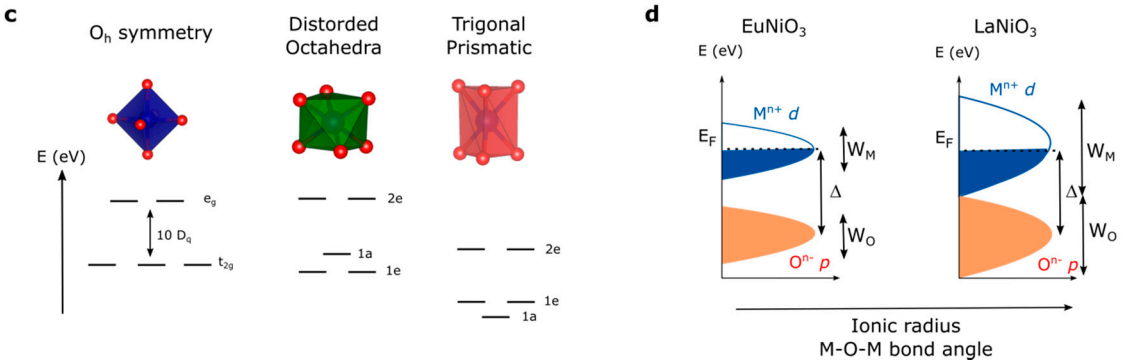

Figure 5. (**a**) Evolution of the perovskite structure following the modification of the Goldschmidt factor. (**b**) Variation of the Madelung constant of oxygen and cobalt compared to the distance Co–O (in Å) in $La_{1-x}Sr_xCoO_3$ (solid lines and full symbols) compared to Li_xCoO_2 (dashed lines and open symbols) for x = 0, 0.5, and 1 corresponding to formal oxidation state of Co^{3+}, $Co^{3.5+}$, and Co^{4+}, respectively. (**c**) Modification of the crystal field from perfect O_h symmetry to distorted octahedral found for orthorhombic, rhombohedral or hexagonal perovskite and trigonal prismatic symmetry found for hexagonal perovskites. (**d**) Modification of the band width for the $RNiO_3$ series by tuning the M–O–M bond angle through the modification of the rare-earth R ionic radius.

5. Reactivity of the Oxygen Species Formed Upon Oxidation

Before describing in greater detail the oxidation processes taking place on the surface of perovskites during OER, we should recall here that bulk oxidation can also take place for perovskites. Hence, owing to the presence of bulk oxygen vacancies and interstitial oxygen sites, bulk oxidation can proceed through the insertion and diffusion of O^{2-} ions into the structure. Following the above description, the charge upon O^{2-} insertion can be compensated either by a cationic redox reaction (electrons removed from MO* states) or by the oxidation of oxygen ions (electrons removed from pure O *p* states). Different charge compensation mechanisms can then be envisaged in the bulk of perovskites upon oxygen insertion, and we refer the readers to more detailed works on these phenomena [57,58]. When removing electron from pure O *p* states in the bulk, unstable oxyl species would be formed prior to stabilization by charge reorganization. While examples have now been given for the structurally more flexible layered compounds used as Li-ion battery positive electrodes [16,18,20], only rare examples describing the reorganization of lattice oxygen reorganization in the perovskite structure can be found. Indeed, due to the rigidity of the corner-shared octahedral arrangement and the relatively large O–O bond distance, this reorganization is foreseen to be almost impossible for cubic perovskites. This is especially true for 3*d* metals for which the covalence of the M–O bond is rather weak compared to 4*d* and 5*d* metals [22,48]. However, when lowering the symmetry in order to accept a local decrease of the O-O distance, some examples can be found in the literature of O–O bond formation for perovskite related compounds. Hence, true peroxo O_2^{2-} groups were reported to be formed in hexagonal perovskites such as $La_{1.2}Sr_{2.7}MO_7$ (M being Ir or Ru) [59] or $Ba_5Ru_2O_{11}$ [60]. Interestingly, these peroxo O_2^{2-} groups can be stabilized owing to electrostatic stabilization with the large and polarizable alkaline-earth Ba^{2+} or Sr^{2+}, in an identical manner to the stabilization of peroxide groups in ionic Li_2O_2 or Na_2O_2 compounds, for instance. Nevertheless, caution must be taken since no $M-O_2^{2-}-M$ bonds are formed for these hexagonal compounds and the electronic configuration will be different from a charge compensation mediated by electron donation to iono-covalent bonds (MO* states).

When considering surface oxidation processes that can take place when an external electrical field is applied, i.e., under electrochemical conditions, several cases can be inferred. When the electrons are removed from oxygen states, electrophilic oxyl groups are formed on the surface through the formation of unpaired electrons, the reactivity of the oxygen being very different from the ligand hole

formed through the removal of electrons from MO* states with a large oxygen character (i.e., covalent M–O bond) and which are delocalized. Indeed, electrophilic oxyl groups can react with a nucleophilic species. This scenario is important when considering the O^{-}/O^{2-} redox couple as a catalytic center.

Indeed, the oxyl groups formed upon oxidation will not only be very reactive to any nucleophilic species, such as water, but also lead to O–O bond formation on the surface, such as discussed for d° $SrTiO_3$ for instance [25]. Both cases would eventually lead to the condensation of gaseous oxygen and result in the formation of oxygen vacancies on the surface. However, when both oxygen and MO* states lie at the Fermi level ($\Delta = U/2$, Figure 4b), the redox reaction is considered to be mixed anionic and cationic. In this case, structural and charge reorganization may occur. This reorganization would distort the oxygen network to accommodate the formation of holes in the oxygen 2*p* states. In this case, the O–O bond distance remains sufficiently large so that the oxygen remains coordinated to the metal and does not condense to form $O_{2(g)}$.

6. Examples of Perovskite Oxygen Oxidation for Catalytic Reactions

After having established electronic factors governing the redox activity of oxygen in perovskite materials, a few examples will be given to demonstrate how the redox process of oxygen ions can be used to enhance the catalytic or electrocatalytic properties of perovskites. In particular, we will discuss the involvement of oxygen as an active site for the OER in aqueous media, and focus the discussion on how this mechanism can lead to the improvement in activity by decreasing the energy barrier for the formation of the O–O bond, as well as inducing drastic instabilities due to charge compensation mechanisms. For comparison, literature reports that employ defect chemistry or "oxygen vacancies" to explain the enhancement of OER activities will also be discussed. Finally, we will briefly explain some classical high temperature gas phase oxidation or reduction reactions that follow a Mars van Krevelen mechanism [61,62]. Throughout these examples, we aim to provide readers with a broad vision of the involvement of surface oxygen into various catalytic reactions, highlighting the understanding built by different research communities.

6.1. Low Temperature Oxygen Evolution Reaction

As illustrated in Figure 3 and discussed previously elsewhere [6,23,28,63], accessing the redox of oxygen in perovskites materials will be possible at low energy corresponding to a potential at which H_2O is usually oxidized to form gaseous oxygen. Therefore, the reactions of interest for which oxygen can be used as an active site are limited. Moreover, some specificity related to surfaces must be recalled before discussing these reactions. Hence, special care must be taken when discussing the surface redox properties of transition metal oxides in light of the bulk electronic structure. Indeed, several works clearly demonstrated that, under vacuum, structural relaxation on the surface of perovskites can lead to a shift in energy of several hundreds of meV for the oxygen states compared to the Fermi level [64–66]. Moreover, when in contact with a solvent, the surface of a transition metal oxide develops an energy that can be in the range of 1–2 J/m^2 [65].

For a long time, the metallic center was believed to be the active site for the OER to proceed on the surface of transition metal oxides. Hence, based on molecular orbital principles, the number of transition metal *d* electrons was discussed by Bockris and Otagawa as one of the simplest electronic descriptors [67,68]. Studying a series of AMO_3 (M = Cr, V, Mn, Fe, Co, Ni) perovskite electrocatalysts, the OER overpotential was found to inversely correlate with the enthalpy of hydroxide formation and with the amount of *d*-electron which is postulated to have a strong influence on the metal–OH* bond strength as well as on the chemisorption of oxygen, as discussed by Dowden et al. [69] and recently computed by Calle-Vallejo et al. [70]. Furthermore, Dowden also argued that the chemisorption could be affected by the crystal field stabilization energy (CFSE) with different e_g occupancy. This assumption was then studied by Shao-Horn and co-workers [71,72], proposing that the OER activity for perovskites follows a volcano shape with the occupancy of the e_g electronic states serving as an activity descriptor. This model based on the e_g occupancy was considered as the first demonstration of

chemisorption trends on the surface of transition metal oxides using a classical coordination chemistry approach. In contrast to the OER descriptor using *d*-electrons suggested by Bockris and Otagawa, the e_g occupancy introduces a difference for the reactivity of orbitals depending on their symmetry, with the σ-interaction of the e_g states dominating over the weaker π-interaction of the t_{2g} states.

Bulk band descriptions of the electronic states can also provide insightful information on the formation of adsorbates on perovskites' surface. Meadowcroft first employed the band structure of oxides as a descriptor in the investigation of perovskites for ORR in the 1970's [73] before Matsumoto and co-workers later postulated that the electron transfer rates for the ORR is determined by the delocalization of the σ* (e_g) states into bands and proposed that the band width of the σ* states, which reflects the electron mobility of the oxide, could be an important descriptor for the oxygen electrocatalysis [9,74]. These early works paved the way to the more recent work on perovskites for which both the σ* (e_g) states and the M–O covalent character were proposed to govern the OER activity on the surface of perovskites [72]. From this description based on MO* states, an important addition to our understanding was made by analogy with the gas phase field for which the energy gap between the O *p*-band center and the Fermi level was shown to correlate with the oxygen surface exchange kinetics [9]. Going further in this direction, the demonstration was made that moving the Fermi level closer to the O *p*-band center of double perovskites $Ln_{0.5}Ba_{0.5}CoO_{3-\delta}$ (Ln = Pr, Sm, Gd and Ho) correlates with the OER activity as well as with the stability of the perovskites for which accessing oxygen states leads to severe surface decomposition such as for $Ba_{0.5}Sr_{0.5}Co_{0.8}Fe_{0.2}O_{3-\delta}$ perovskite or as recently demonstrated for manganites [66,75–77].

Realizing that the position of the oxygen *p* states compared to the Fermi level correlates not only with the OER activity but also with the stability of the perovskites surface, challenges the commonly accepted mechanism based on oxygen adsorption on a metallic site. Although computational works [5,7] have proposed a mechanism mediated by the formation of surface oxygen vacancies, limited experimental evidence has been provided so far due to the lack of proper techniques to capture the transient nature of surface intermediates. Recently, combining oxygen isotopic labelling and in situ mass spectrometry, the demonstration was made that using negative charge transfer materials such as $SrCoO_3$ leads to the participation of the lattice oxygen in the OER reaction (Figure 6) [6]. Similar lattice oxygen involvement was also proposed for the same materials by Stevenson et al. [5]. Interestingly, no lattice oxygen was found to be evolved for $SrFeO_3$ for which the charge transfer is null. Therefore, special care must be taken when using bulk electronic properties to describe the surface reactivity and the electrocatalytic activity of perovskites, and further understanding must be developed. Moreover, even if a correlation has been found between the OER activity and the involvement of surface oxygen for cobalt-based perovskites, this does not preclude from finding transition metal oxides demonstrating large OER activity with the metal acting as the catalytically active center. Hence, efforts must be made to understand and rationalize the energetics relating to the different mechanism. Nevertheless, some interesting points can be inferred from these studies. First, switching from transition metal to oxygen as active site is eventually accompanied by a change in rate determining steps from the O–O bond formation to a deprotonation step. This could be explained by the large reactivity of surface oxyl groups with water that eventually lowers the energy barrier for the O–O bond formation. Interestingly, the switch in rate determining step to a deprotonation step was also proposed for perovskites by computational works [7,78]. However, since a chemically limiting step related to proton transfer was found when triggering the involvement of surface oxygen during the OER [23,78], it precludes the use of the so-called hydrogen reference electrode, commonly employed to estimate and scale the energetics of the reaction intermediates so as to obtain a thermodynamical overpotential [78,79]. Therefore, the design of perovskite catalysts with surface active oxygen, calls for the development of dedicated computational tools in order to better understand these complex mechanisms. Moreover, $LaNiO_3$ perovskite, previously discussed as a potential charge transfer material (Figure 5d), was also proposed by computation to involve surface oxygen as the active site [7]; even though this compound

was previously studied for its propensity for diffusion of oxygen vacancies [80], this assertion remains to be experimentally demonstrated.

At this point, the different mechanisms proposed in the literature for surface oxygen involvement in the OER reaction must be compared. The first one, designated in the literature as the lattice oxygen mechanism (LOM) [5,7], proposed the formation of an O–O bond from the reaction of a bridging oxygen with a dangling deprotonated oxygen. The second mechanism invoked the formation of an O–O bond by the reaction of OH^- from the electrolyte with deprotonated oxygen atoms. Interestingly, when performing in situ mass spectrometry on ^{18}O-labeled perovskites, two type of gaseous oxygen were found: $^{34}O_2$ coming from the reactivity of one oxygen from the electrolyte with lattice oxygen and $^{36}O_2$ arising from the combination of two lattice oxygens [6]. Therefore, it is critical to further understand the electronic states respectively involved in these two types of O–O bond formation, denoted respectively acid-base and direct coupling reactions by the homogeneous catalysis community [81,82]. One can however tentatively propose that the acid-base reaction would be preferentially triggered by the oxidation of pure oxygen states and the formation of oxyl groups on the surface, as the electrophilic oxyl groups would react with nucleophilic species such as lone pairs from water molecules. Nevertheless, further understanding of the mechanisms triggered by the oxidation of oxygen ions on the surface of perovskites and their respective kinetics remains an urgent task.

Realizing that lowering the chemical potential of the transition metal is necessary to access the oxygen *p* states and enhance the OER kinetics, perovskites with higher oxidation states were thereafter envisioned as OER catalysts. For that, different synthetic approaches were employed. The first one consists of using chemical pressure induced by the partial replacement of the transition metal by a large alkaline cation such as Li^+ or a rare earth cation in order to stabilize the 5+ oxidation state [83,84]. For instance, using La_2LiIrO_6 as a model compound, it was proposed that Ir^{5+} is inactive for the OER in alkaline media, and that further oxidation/delithiation in acids was necessary to oxidize the surface oxygen, which then becomes electrophilic and prone to react with water, thus eventually enhancing the OER kinetics [23]. When doing so, drastic surface reconstruction arising from the lowering of the coordination of the metal due to the formation of oxygen vacancies was observed, and also reported for $SrIrO_3$ and $SrRuO_3$ upon oxidation from Sr^{2+} chemical leaching [85,86]. Hence, using surface oxygen as active site eventually induces the formation of surface oxygen vacancies, which can be compensated for by the formation of cationic defects and the dissolution of surface cations if the rate of oxygen insertion from the aqueous electrolyte is not fast enough. Moreover, the formation of surface oxygen vacancies can also be counterbalanced by the migration of lattice oxygen to the surface, as visualized by high resolution transmission electron microscopy (HRTEM) and also spotted by online electrochemical mass spectroscopy (OLEMS) (Figure 6a–e) [6,23]. Finally, other perovskites containing Ir^{5+} were recently proposed as highly active OER catalysts in acidic conditions without further mention being made of their surface stability [84]. Further work is thus needed to assess if Ir^{5+} based perovskites can indeed be active, or if surface degradation is also encountered. Finally, to avoid the corrosion of perovskites under oxidative conditions, the rate of surface vacancies refilling must compete with the rate of oxygen vacancies formation, for which nothing is known as yet. If the kinetics of surface vacancies refilling is slower than the kinetics associated with oxygen vacancies formation, as suggested by the pH dependence observed for $SrCoO_3$ compounds for instance, under-coordinated sites prone to either dissolution or reconstruction will be formed on the surface. Hence, recent thermodynamical calculations suggested transition metal oxides as being universally unstable under OER conditions [87]. However, these calculations neither take into account specific interactions with water and counterions on the surface [88], nor reflect the orientation dependence for the stability of the oxides [89], as reported for $SrRuO_3$ perovskites for instance [86], which can largely modify the stability of transition metal oxides under OER conditions. Nevertheless, as a general trend, while triggering surface oxygen as an active site for OER might be seen as a blessing due to the enhanced OER kinetics, drastic instabilities must be anticipated.

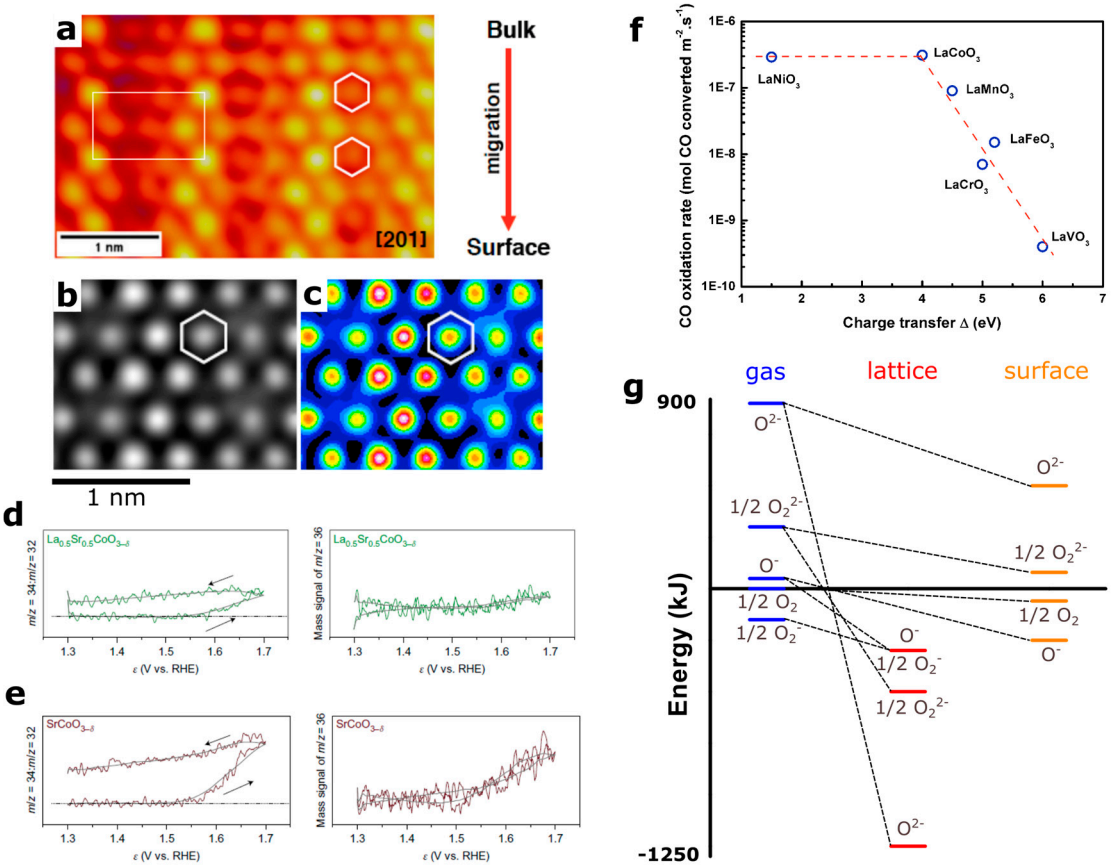

Figure 6. (**a**,**b**) High resolution transmission electron microscopy (HRTEM) images showing lattice migration (iridium and oxygen) for La_2LiIrO_6 induced by surface oxygen reactivity during oxygen evolution reaction as well as (**c**) simulated HRTEM images [23]. (**d**,**e**) on-line mass spectrometry (OLEMS) profile for $^{34}O_2$ and $^{36}O_2$ oxygen species measured for $La_{0.5}Sr_{0.5}CoO_{3-\delta}$ and $SrCoO_{3-\delta}$ labelled with ^{18}O isotope during oxygen evolution reaction in $H_2{}^{16}O$, demonstrating the involvement of lattice oxygen in the oxygen evolution reaction (OER) reaction [6]. (**f**) CO oxidation rate as reported by Tascon et al. as a function of charge transfer energy for $LaMO_3$ series [90]. (**g**) energy diagram of various oxygen species in gas phase, solid phase and at the surface of binary oxides as reported by Bielanski and Haber and further refined by Bouwmeester et al. [64]. Adapted from Ref. [6,23], Nature Publishing Group (**a**–**e**) and from Ref. [64] Elsevier (**g**).

Another synthetic strategy to stabilize perovskite materials with higher oxidation state and therefore lower the chemical potential of the metal is to use physical pressure, as extensively studied by Demazeau et al. for La_2LiMO_6 perovskites [91–93]. For instance, Yagi and coworkers stabilized using high pressure synthesis Fe^{4+} into the charge transfer quadrupole perovskite $CaCu_3Fe_4O_{12}$ and demonstrated its large OER activity [94]. Owing to the short O–O bond distance (≈2.6 Å) stabilized by the use of high pressure synthesis, the direct O–O bond formation between two neighboring lattice oxygen was proposed to be a possible reaction intermediate for the formation of gaseous oxygen. If confirmed, the direct formation of an O–O bond within the structure of quadrupole perovskites would be of great interest, and would confirm measurements made on $SrCoO_3$ showing that direct coupling of two lattice oxygen is a possible pathway for OER [6]. This approach shows promise not only in terms of activity, but also in terms of stability as it provides a unique way to nearly suppress the use of basic alkaline-earth cations that are prone to leach out in alkaline solution or in contact with water [53,77,95,96], as recently spotted by in situ TEM for $Ba_{0.5}Sr_{0.5}Co_{0.8}Fe_{0.2}O_{3-\delta}$ [75].

So far, throughout the series of perovskites reported as water splitting catalysts, it can be envisaged that when the Fermi level enters into the oxygen states, surface oxygen and eventually lattice oxygen,

by migration, take part in the OER reaction. Nevertheless, experimentally the formation of reactive oxygen can only be captured by detecting O_2 gas evolution from the bulk perovskites and from lattice distortion or from the formation of defects induced by the participation of surface oxygen. Although we now understand when oxygen electronic states are involved in the redox process by using bulk electronic structure, the exact nature of the surface oxygen states under OER conditions remains largely unknown. Even though the development of adapted tools allowed for the detection of the involvement of oxygen as redox center, efforts still need to be made to further describe and visualize the intermediates of the reaction.

On the other hand, over the past several years, tremendous efforts have been devoted to understanding surface defect chemistry under OER conditions, and to identify correlations between the oxygen vacancies formation and the observed high OER activity for some model perovskites. Considering $SrCoO_3$ for example, DFT calculations proposed that the diffusion of O* into oxygen vacancies is thermodynamically and kinetically feasible for different O* coverages, implying that surface oxygen vacancies will be annihilated during the adsorption and buildup of O*. It was therefore proposed that filling of surface oxygen vacancies occurs during oxygen incorporation at a fraction of the generated atomic oxygen in the first few steps of the oxygen evolution reaction. Absorbed oxygen can then diffuse without a barrier into empty surface vacant sites, thus annihilating the vacancies which were shown to be detrimental to the overall OER [97]. However, severe degradations leading to surface amorphization may simultaneously occur due to the oxygen vacancy formation at the surface. Eventually, the stability of such catalysts would be a compromise, except when oxygen refilling is fast enough or if a self-healing mechanism with a constant dissolution/deposition process can be controlled. Jooss et al. [76] investigated the defect chemistry in the active states of a series A-site doped $Pr_{1-x}Ca_xMnO_3$-H_2O interface, and revealed interesting correlations between activity, stability, and changes in the electronic band structure induced by doping. The most favorable electrocatalytic properties are shown in the substitution range of $0.3 \leq x \leq 0.5$, where the hole carriers have mixed Mn 3*d* and O 2*p* character, and can establish the most efficient charge transfer across the PCMO-H_2O interface. Further X-ray photoelectron spectroscopy (XPS) and X-ray absorption (XAS) studies at the Mn L- and O K-edges showed that a reduced Mn^{2+} species is generated at the catalyst surface under the oxidizing conditions of the OER. Hence, oxygen vacancies are formed according to $Pr_{1-x}Ca_xMn^{3+x}O_3 + 2e \leftrightarrow Pr_{1-x}Ca_xMn^{2+x}O_{2.5} + V_{\ddot{O}} + \frac{1}{2}O_2$ at a redox potential of E^0 (Mn^{4+}/Mn^{2+}) = 1 V vs. SHE. Interestingly, the decomposition kinetics is also strongly affected by the defect chemistry of the catalyst in its active state. It was then observed that the degradation via recrystallization and amorphization in Ca-rich samples is accompanied by Ca^{2+} depletion from the reacted zones, similarly to the report on $SrIrO_3$ in acidic conditions. Moreover, subtle band structure effects such as the splitting of the Mn 3*d* e_g states and changes in the character of the hole states were proposed to have an impact on charge transfer during water oxidation and may govern if the oxygen vacancies formation is assisting by catalysis or by a corrosion process. Finally, the best example of cations leaching is given for vacancy-containing $Ba_{0.5}Sr_{0.5}Co_{0.8}Fe_{0.2}O_{3-\delta}$ (BSCF) which is thermodynamically predicted as unstable and expected to decompose at relatively low temperatures into a mixture of several cubic and hexagonal perovskite phases, [11] and further experimentally confirmed [77,96]. Eventually, Han et al. directly visualized the formation of gaseous O_2 during the incorporation of H_2O into the lattice of BSCF where dramatic structural oscillations were observed by in situ environmental transmission electron microscopy (ETEM) [75].

As a conclusion, at this stage of our understandings, when studying new perovskites as OER catalysts, extreme caution must be taken in order to accurately determine if the surface undergoes corrosion and drastic reconstruction under oxidation conditions. Indeed, the stabilization of non-equilibrium concentrations of defects in the active state of the catalyst without corrosion is of high importance for the future optimization of OER catalysts with enhanced activity.

6.2. Gas Phase Catalytic Reaction

The oxygen defect chemistry for bulk perovskites is well-known and has been largely studied for high temperature catalytic reactions. Hence, it is no surprise that perovskites recently studied for the OER reaction have been previously investigated as mixed ionic electronic conductors (MIEC) for SOFC [98] or as catalysts for various reactions such as hydrocarbons oxidation, SO_2 oxidation, CO oxidation, NO reduction, and others [99–101]. We hereby provide the reader with general information on perovskites used as high temperature catalysts. We do not aim to provide a full review of these properties, but rather shed light on the basic understanding of the reactivity of lattice oxygen through discussion of a few examples in order to show some similarities in trends between the water splitting reaction in aqueous media and the high temperature catalytic processes in the gas phase.

While the understanding of surface oxygen participation to the OER is still in its infancy, several types of oxygen species have been identified on the surface of perovskites and their respective catalytic activity extensively discussed. Hence, in the 1970s Voorhoeve et al. proposed that oxidation and reduction reactions on the surface of perovskites could be classified into two categories: suprafacial and intrafacial reactions [99,100]. The reaction between adsorbed species on the surface of perovskites, described as suprafacial reaction, proceeds at relatively low temperatures while the intrafacial reaction is a high temperature process in which the reaction rate is correlated with the thermodynamic stability of lattice oxygen (enthalpy of formation of vacancies, as shown in Figure 4e). Yamazoe et al. further investigated the nature of surface oxygen species for the $La_{1-x}Sr_xCoO_{3-\delta}$ series by using temperature programmed desorption (TPD) and X-ray photoelectron spectroscopy (XPS) techniques [102]. Large amounts of oxygen were measured by TPD to desorb between room temperature and 850 °C, first with a broad desorption peak denoted α-O below 700 °C followed by a sharp desorption peak at ca. 820 °C and denoted β-O. Furthermore, a doublet was found for most of the studied perovskites in the O1s XPS spectra: the peak at lower binding energy (528.2 eV) was assigned to lattice oxygen when the second contribution at higher binding energy (530.2–531.4 eV) was attributed to adsorbed oxygen on the surface and was found to be dependent on the nature of the transition metal. From both desorption and spectroscopic measurements, it was thus concluded that α-O was surface adsorbed oxygen while β-O was lattice oxygen. Building upon these early works, the complexity of these oxygens were further uncovered and their dependence on the chemistry of the perovskites thoroughly discussed [103–106].

Since different types of oxygen species (α-O for surface adsorbed oxygen, α1-O for surface lattice oxygen in interstitial space, and β-O for lattice oxygen in the bulk crystalline) co-exist for perovskites, oxidation of hydrocarbons by molecular oxygen can be either governed by a suprafacial or an intrafacial mechanism. The suprafacial mechanism prevails at low temperature (100–400 °C) when the lattice oxygen becomes mobile and therefore active by increasing the temperature, hence it gradually transitions to an intrafacial mechanism. Even if no direct correlation can be made between the enthalpy of formation of surface oxygen vacancies compared to the enthalpy of formation of bulk oxygen vacancies, interesting trends are found. Following a classical Mars van Krevelen type mechanism for which oxygen from the catalyst participates in the catalytic reaction [61], the following two step mechanism can be proposed for the oxidation of a gas such as CH_4:

reaction of the reactant with oxygen from the transition metal oxide:

$$CH_{4(g)} + O_O^{\times} \rightarrow CO_{(g)} + 2H_{2(g)} + V_O^{\cdot\cdot} + 2e'$$

followed by the reoxidation of the reduced catalyst by gaseous oxygen:

$$V_O^{\cdot\cdot} + \frac{1}{2}O_{2(g)} + 2e' \rightarrow O_O^{\times}$$

Therefore, this two steps mechanism is in part governed by the enthalpy of formation of oxygen vacancies for perovskites which can, following a linear free energy relationship [107], eventually

govern the kinetics of the oxidation reaction. Hence, bulk properties have been used to describe the kinetics rate constant for various gas oxidation or reduction reactions on the surface of perovskites. For instance, the catalytic activity of $LaMO_3$ perovskites for CO oxidation as reported by Tascon et al. can be correlated with the bulk charge transfer energy Δ in Figure 6f [90], owing to the direct correlation existing between the enthalpy of formation of oxygen vacancies and the charge transfer energy Δ as shown in Figure 4e.

In a similar manner, the oxygen surface exchange coefficient, which is critical for the oxygen reduction reaction on the surface of SOFC cathodes, was also found to correlate with the charge transfer energy (or the energy of the oxygen *p* states) [9]. In the research field of SOFC, one is well aware of the possibilities given by the formation of oxygen vacancies [9,12,46,47] and surface oxygen exchange. Two mechanisms have been uncovered for the oxygen reduction reaction. The first one proceeds by the $O_{2(g)}$ adsorption and first electron transfer to form O_2^-. Then, the $O_2{}^-$ adsorbed species are dissociated into two O^- bonded to surface transition metals. Finally, O^- meets with surface oxygen vacancies to be further reduced and form lattice O^{2-} (denoted O_O^x using the Kroger-Vink notation). In a simplified way, the overall reaction can be written as follows:

$$O_{2(g)} + e^- = O^-_{2(ads)}$$

$$O^-_{2(ads)} + e^- = O^{2-}_{2(ads)}$$

$$O^{2-}_{2(ads)} = 2O^-_{(ads)}$$

$$O^-_{(ads)} + V_O^{\cdot\cdot} + e^- = O_O^x$$

Following this mechanism, the main intermediates are therefore the adsorbed O_2^{2-} and O^-, which are incorporated into surface oxygen vacancies to form O^{2-}. In this case, the mechanism is mediated by the mixed valence states of the transition metal cations and the surface migration of O^- and oxygen vacancies. Possibly, oxygen states are not oxidized in the lattice of the oxide materials and the redox process would be described as cationic for the transition metal oxide. The second mechanism is mediated by surface vacancies with first the adsorption of $O_{2(g)}$ directly into surface vacancies followed by its reduction to form O_2^{2-} species. The dissociation of O_2^{2-} species then leads to the formation of two different O^- species: one formed in the lattice which could be described as O_O and another one adsorbed on the surface ($O^-_{(ads)}$). Finally, O_O is further reduced and $O^-_{(ads)}$ meets with a surface oxygen vacancy, both leading to the formation of O_O^x. As the vacancy mechanism involves the oxidation of surface oxygen species (different from adsorb), the redox activity of oxygen ions is necessary for this mechanism to be triggered. Different reviews have been dedicated to this topic [9,10,13], which is not the focus of this review.

6.3. Concluding Remarks on Using Redox Reactions of Oxygen Ions for Catalysis

Through these different examples, it appears that while it is well-accepted in the high temperature catalysis community that surface oxygen is easier to oxidize than bulk oxygen and that both can be used as reactive sites, everything still remains to be done to understand and control the participation of oxygen as an active site for the OER. This is especially true knowing that numerous types of adsorbed or surface oxygen species may exist, as depicted by the energy diagram proposed by Bielanski and Haber and reproduced in Figure 6g [64,108]. Nevertheless, similarities between both fields can easily be seen, for instance when comparing the adsorption of gaseous oxygen for $LaMO_3$ series with their ORR performances in Figure 7 [71,90]. Indeed, gradually increasing the amount of *d* electrons in perovskites, *p*-type semi-conductors or even metallic perovskites can be formed, the surface of which will be able to donate electrons for the absorption of oxygen species. In this case, surface adsorbed oxygen species will behave as electrophilic centers and oxidative reactions are expected to occur through the nucleophilic attack of the reactant. Hence, peroxo (O_2^{2-}) or superoxo (O_2^-) species are

likely to be formed as intermediates during the reaction [64,82]. However, heterogeneous catalysis at a solid/liquid interface is rather complex and the nature of the surface oxygen species can largely differ depending on the solvent, applied potential, surface termination, and other parameters [15,18]. A first example is given by the pH of zero charge which is known to increase for perovskites with the covalent character of the M–O bond [67], eventually modifying the protonation state of the terminal oxygen. Moreover, the energetics of charged surface oxygen species can be greatly modified by charge transfer with the solvent, i.e., water for the OER, due to chemical potentials alignment. Furthermore, hydrogen bonds between adsorbed species and water molecules, but also within water molecules in the Helmholtz plan, can influence the reaction pathway. Therefore, everything remains to be done to understand the role of surface active oxygen species for electrocatalytic reactions in water and their exact nature. For this, not only dedicated approaches but also new analytical tools must be developed, which will be discussed in the following section.

Finally, nothing is known so far about the competition between the surface reaction and the diffusion processes from the bulk to the surface for OER catalysts, but knowledge can be taken from high temperature bulk diffusion studies. Indeed, the surface of perovskites is far from equilibrium during the OER, and defects are constantly formed and refilled. While the diffusion from the solution to the surface might be considered fast, almost nothing is known concerning the diffusion from the bulk to the surface of the catalyst in order to counterbalance the charge defects. Hence, being able to determine the kinetics of surface reactions, corrosion, as well as bulk diffusion is of prime importance for assessing the stability of perovskite-based OER catalysts.

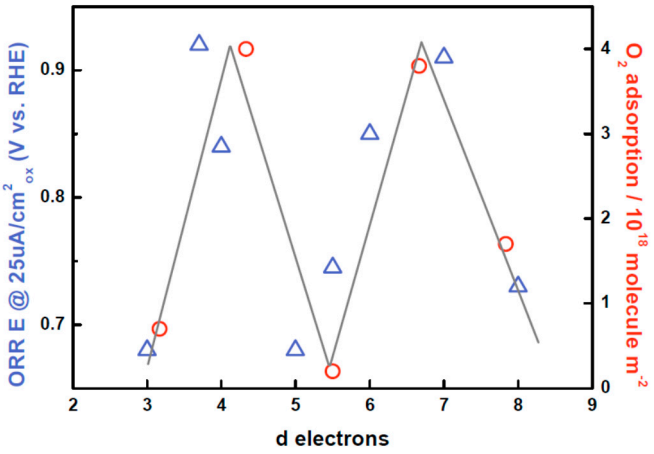

Figure 7. Oxygen reduction reaction activity (at 25 μA/cm$^2_{oxide}$) as reported by Suntivich et al. as well as reversible oxygen adsorption at P = 150 mmHg and T = 298 K as reported by Tascon et al., both as a function of *d* electrons for the $LaMO_3$ series [71,90]. Both curves show the characteristic M shape as a function of *d* electrons, demonstrating that oxygen adsorption properties at a solid/gas and at a solid/liquid interface are correlated for a given series of transition metal oxides.

7. Latest Development of Analytical Tools for Analyzing the Oxidation Reaction of Oxygen Ions

The visualization and the identification of lattice oxygen oxidation for perovskites in bulk or on the surface have always been challenging, and the development of new analytical tools and strategies is very much required. Owing to the unstable nature of oxygen species formed upon oxidation and their large reactivity described above, these species are by nature transient and can be detected either thanks to their reactivity or thanks to the structural reorganizations that their formations trigger. Many techniques, such as in situ environmental transmission electron microscopy (ETEM), transient infrared spectroscopy, (NMR), X-ray absorption spectroscopy (XAS), online electrochemical mass spectroscopy (OELMS), have been recently employed to identify the redox-active centers on the surface of perovskite oxides (Figure 8).

The first tools to come to mind are the X-ray absorption and emission spectroscopy techniques (XAS and XES, respectively). Hence, by coupling XAS measurements at the metal K-edge and at the oxygen K-edge, the holes formed on a greatly covalent M-O bond can easily be spotted [35,37,77]. Indeed, no energy shift at the metal K-edge is observed while the pre-edge feature at the O K-edge probing the transition from O 1*s* core level to the hybridized O 2*p*/M 3*d* states increases, indicating an increased oxygen character for the MO* states (i.e., an increased covalence of the M–O bond). However, holes formed on non-bonding oxygen *p* states are hard to spot, and only new states related to the formation of O–O bonds are usually detected by XAS at the O K-edge. Unfortunately, as discussed previously, this scenario is rare and no such O–O states have been observed so far for perovskites, in contrary to layered compounds used as Li-ion battery materials [18]. To demonstrate the redox activity of surface oxygen anions in oxygen-deficient iron-based perovskites used as SOFC materials, operando X-ray absorption spectroscopy was used by Mueller and coworkers [15]. Combining soft XAS at the O K-edge and the metal L-edge, the oxygen surface exchanged was found to be associated with the oxidation of surface oxygen while the oxygen adsorbate is reduced. This complex redox process was explained by the electron donation of adsorbed oxygen species to unoccupied oxygen *p* states. Hence, this observation confirmed that surface oxygen on perovskites is a significant redox partner to the oxygen adsorbate during electrochemical reactions. Nevertheless, while in situ XAS techniques seem well adapted for the study of high temperature solid/gas interface or solid/liquid interface for amorphous films for which the whole thickness is active, limits in sensitivity might hamper its use for the study of transient states on the surface of bulk material in contact with water and a dedicated approach must be developed.

As discussed before, the recent development of in situ environmental TEM (ETEM) offers a unique opportunity to visualize the reactivity of oxidized surface oxygen and the surface reconstructions triggered by this phenomenon. The demonstration of the potentiality of ETEM was recently given by Jooss and co-workers who developed a combined ETEM and ex situ cyclic voltammetry approach to study the oxygen evolution on the surface of $Pr_{1-x}Ca_xMnO_3$ compounds [76,109]. Injecting a mixture of SiH_4/H_2O/He into the TEM sample chamber, the electron beam illumination on a crystalline $Pr_{1-x}Ca_xMnO_3$ sample was found to induce O_2 evolution and the immediate growth of an amorphous SiO_{2-x} layer (Figure 8). For low calcium content ($0.3 \leq x \leq 0.5$), the solid SiO_{2-x} surface selectively grows on top of the active crystalline surface but not on amorphous areas, whereas for $Pr_{1-x}Ca_xMnO_3$ compounds with high calcium concentration ($x \geq 0.75$) the surface undergoes a drastic corrosion process, hence demonstrating two competing reactions on the surface of Mn-based perovskites. Coupled with density of states calculations, the catalysis of the $Pr_{1-x}Ca_xMnO_3$ compounds was then explained in terms of band structure, and especially charge transfer ($\Delta < U$) vs. Mott insulator regime ($\Delta > U$), with the optimal catalyst having mobile carriers with a mixed metal *d* and oxygen *p* character, as we previously described in Figure 4 for the case $\Delta = U/2$. A very recent work further confirmed using ETEM the correlation existing between electronic structure and reactivity with water under beam illumination for the $La_{1-x}Sr_xCoO_{3-\delta}$ series and $Ba_{0.5}Sr_{0.5}Co_{0.8}Fe_{0.2}O_{3-\delta}$ [76]. Direction visualization of lattice breathing and O_2 bubble formation was provided for perovskites having the oxygen *p* states close to the Fermi level, while this phenomenon was not observed for perovskites such as $LaCoO_3$ that show a purely cationic redox reaction.

Solid-state NMR spectroscopy can also provide useful information to clarify the local structure and the dynamics of oxygen ions induced by their migration from the bulk to the surface upon oxidation. High-resolution ^{17}O solid-state NMR was therefore employed by Grey and co-workers to explore the structural and mechanistic details of the oxygen transport in the paramagnetic $La_2NiO_{4+\delta}$ Ruddlesden-Popper mixed ionic electronic conductor (Figure 8) [110]. Three distinct oxygen environments were identified and assigned to interstitial (O_i), axial (O_{ax}). and equatorial (O_{eq}) sites. Owing to the very high sensitivity of NMR to hyperfine interactions, it might offer a unique opportunity to study the different oxygen environments that can result from the oxidation of lattice oxygen.

Finally, electron paramagnetic resonance spectroscopy (EPR) could be a technique of choice when looking for the formation of holes in oxygen states. However, while EPR was previously used to study high temperature catalysts [64], little has been done so far for heterogeneous electrocatalysts. This is explained by the difficulties related to the presence of EPR non-silent transition metals as well as issues in preparing appropriate samples.

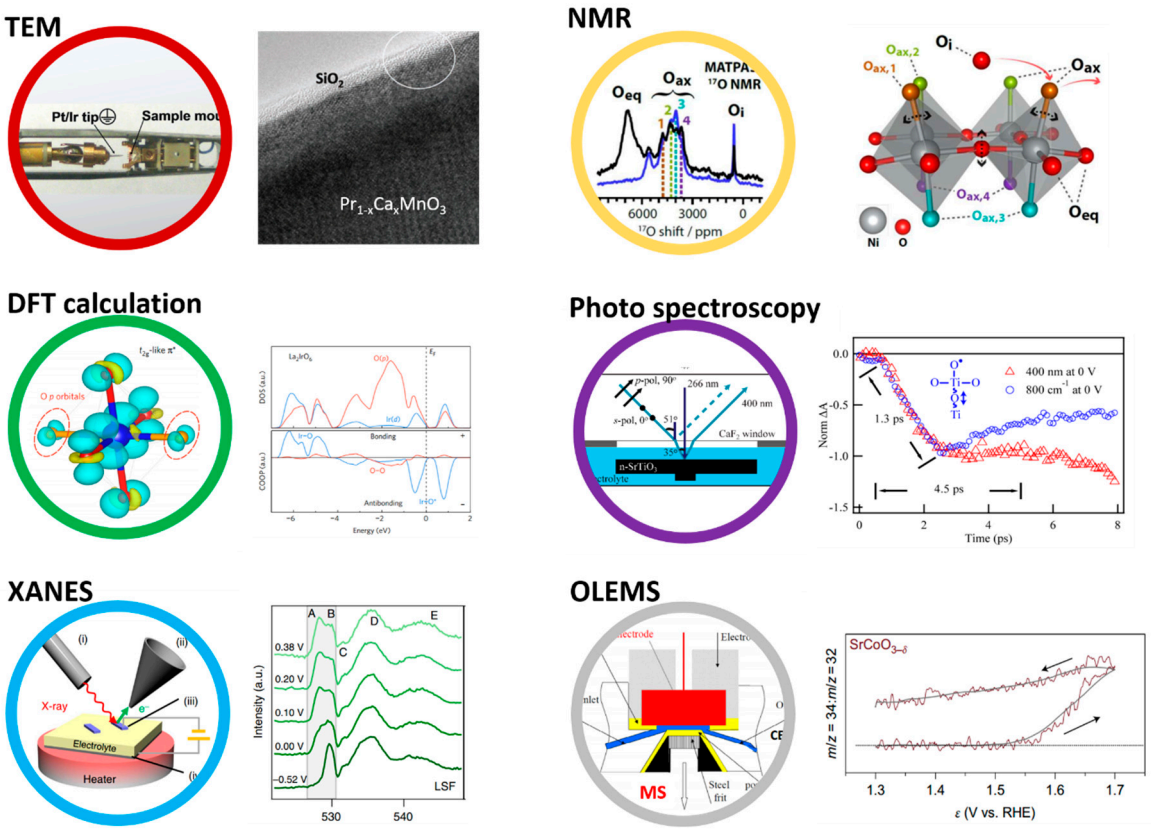

Figure 8. Overview of the different techniques that had being employed to study the redox activity of oxygen in perovskite, including environmental transmission electron microscopy (ETEM), ^{17}O solid-state NMR, density functional theory calculations, ultra-fast infrared photo spectroscopy, operando X-ray absorption spectroscopy (XAS), and online electrochemical mass spectroscopy (OLEMS). Figure adapted from Ref. [6,15,23] from Nature Publishing group, Ref. [27,109,110] from ACS.

Indirect detection of surface oxygen oxidation can also be of great interest. For instance, being able to track the intermediates such as M–O$^{\cdot}$ radical or M=O species formed upon oxidation would have a significant impact on mechanistic understanding of the OER process. As previously mentioned, femtosecond time-resolved infrared spectroscopy has been demonstrated as a successful tool to indirectly track the formation of M–O$^{\cdot}$ or M–O$^{\cdot}$–M radicals [26,27]. Indeed, ultrafast vibrational spectroscopy can identify unique sub-surface vibrations for $SrTiO_3$ involving the stretching of the Ti–O bonds directly induced by the photo-generated Ti–O$^{\cdot}$ oxyl radical on the outermost surface. The detection of unique vibrational modes could prove to be a new tool of interest to monitor the water oxidation reaction at the molecular levels.

Finally, on-line gas analysis coupled with oxygen isotopic labelling was proven to be the tool of choice to provide conclusive evidence for lattice oxygen involvement in catalytic reactions, not only for high temperature [107] but also for low temperature electrocatalytic oxygen evolution [6,111–113], and to explore reaction mechanisms and gain further insight into intermediates formed during the reaction.

8. Conclusions

Through this review, we have tried to demonstrate that we are only scratching the surface of the possibilities arising from the activation of the redox chemistry of oxygen in perovskites used as OER catalysts. While the physical understanding of this phenomenon is now well accepted, only a few compounds have been so far experimentally demonstrated with oxygen as active site for OER. Although using the ZSA formalism we explained that charge transfer materials are required to access oxygen *p* states, very few of them are known and efforts must be made to identify and synthesize new perovskites with oxygen states at the Fermi level. Moreover, open questions remain concerning the stabilization of the oxygen radicals that are formed on the surface under oxidative conditions. Hence, there is no doubt that the development of new analytical techniques is required to better understand the formation of the O–O bond on the surface of the materials during OER. Only dedicated tools will unlock the full potential for activating surface oxygen to improve the catalytic properties of perovskites. While valuable insight can be obtained from computational work on the electronic structure of the bulk of perovskites, understanding the surface reactivity of the oxidized species formed upon oxidation calls for the development of dedicated computational methodologies. This is especially true when considering a solid/liquid interface, for which not only the surface termination, but also the interactions with solvent molecules as well as the applied potential must be considered. Finally, in this review, through comparison with high temperature solid/gas interfaces for which active surface oxygens have been discussed for decades, we hope that a better understanding of the liquid/solid interface can be developed in the near future.

Acknowledgments: The authors acknowledge funding from the European Research Council (ERC) (FP/2014)/ERC Grant-Project 670116-ARPEMA. The authors would like to thank Matthieu Saubanère and Marie-Liesse Doublet, ICGM AIME Montpellier, for fruitful discussions as well as Jean-Marie Tarascon, Collège de France Paris, for his support and fruitful discussions.

Conflicts of Interest: The authors declare no conflict of interest.

References

1. Goodenough, J.B. Perspective on Engineering Transition-Metal Oxides. *Chem. Mater.* **2014**, *26*, 820–829. [CrossRef]
2. Goodenough, J.B. Theory of the Role of Covalence in the Perovskite-Type Manganites [La,M(II)]MnO_3. *Phys. Rev.* **1955**, *100*, 564–573. [CrossRef]
3. Rondinelli, J.M.; May, S.J.; Freeland, J.W. Control of octahedral connectivity in perovskite oxide heterostructures: An emerging route to multifunctional materials discovery. *MRS Bull.* **2012**, *37*, 261–270. [CrossRef]
4. Bednorz, J.G.; Müller, K.A. Condensed Matt Possible High Tc Superconductivity in the Ba-La-Cu-O System. *Z. Phys. B Condens. Matter* **1986**, *64*, 189–193. [CrossRef]
5. Mefford, J.T.; Rong, X.; Abakumov, A.M.; Hardin, W.G.; Dai, S.; Kolpak, A.M.; Johnston, K.P.; Stevenson, K.J. Water electrolysis on $La_{1-x}Sr_xCoO_{3-\delta}$ perovskite electrocatalysts. *Nat. Commun.* **2016**, *7*, 11053. [CrossRef] [PubMed]
6. Grimaud, A.; Diaz-Morales, O.; Han, B.; Hong, W.T.; Lee, Y.-L.; Giordano, L.; Stoerzinger, K.A.; Koper, M.T.M.; Shao-Horn, Y. Activating lattice oxygen redox reactions in metal oxides to catalyse oxygen evolution. *Nat. Chem.* **2017**, *9*, 457–465. [CrossRef] [PubMed]
7. Rong, X.; Parolin, J.; Kolpak, A.M. A Fundamental Relationship between Reaction Mechanism and Stability in Metal Oxide Catalysts for Oxygen Evolution. *ACS Catal.* **2016**, *6*, 1153–1158. [CrossRef]
8. Lee, Y.-L.; Kleis, J.; Rossmeisl, J.; Morgan, D. Ab initioenergetics of $LaBO_3$(001) (B = Mn, Fe, Co, and Ni) for solid oxide fuel cell cathodes. *Phys. Rev. B* **2009**, *80*, 224101. [CrossRef]
9. Lee, Y.-L.; Kleis, J.; Rossmeisl, J.; Shao-Horn, Y.; Morgan, D. Prediction of solid oxide fuel cell cathode activity with first-principles descriptors. *Energy Environ. Sci.* **2011**, *4*, 3966. [CrossRef]

10. Kuklja, M.M.; Kotomin, E.A.; Merkle, R.; Mastrikov, Y.A.; Maier, J. Combined theoretical and experimental analysis of processes determining cathode performance in solid oxide fuel cells. *Phys. Chem. Chem. Phys.* **2013**, *15*, 5443. [CrossRef] [PubMed]
11. Kuklja, M.M.; Mastrikov, Y.A.; Jansang, B.; Kotomin, E.A. The Intrinsic Defects, Disordering, and Structural Stability of $BaxSr_{1-x}Co_yFe_{1-y}O_{3-\delta}$ Perovskite Solid Solutions. *J. Phys. Chem. C* **2012**, *116*, 18605–18611. [CrossRef]
12. Mastrikov, Y.A.; Merkle, R.; Kotomin, E.A.; Kuklja, M.M.; Maier, J. Formation and migration of oxygen vacancies in $La_{1-x}Sr_xCo_{1-y}Fe_yO_{3-\delta}$ perovskites: Insight from ab initio calculations and comparison with $Ba_{1-x}Sr_xCo_{1-y}Fe_yO_{3-\delta}$. *Phys. Chem. Chem. Phys.* **2013**, *15*, 911–918. [CrossRef] [PubMed]
13. Kim, Y.-M.; He, J.; Biegalski, M.D.; Ambaye, H.; Lauter, V.; Christen, H.M.; Pantelides, S.T.; Pennycook, S.J.; Kalinin, S.V.; Borisevich, A.Y. Probing oxygen vacancy concentration and homogeneity in solid-oxide fuel-cell cathode materials on the subunit-cell level. *Nat. Mater.* **2012**, *11*, 888–894. [CrossRef] [PubMed]
14. Lu, Q.; Chen, Y.; Bluhm, H.; Yildiz, B. Electronic Structure Evolution of $SrCoO_x$ during Electrochemically Driven Phase Transition Probed by in Situ X-ray Spectroscopy. *J. Phys. Chem. C* **2016**, *120*, 24148–24157. [CrossRef]
15. Mueller, D.N.; Machala, M.L.; Bluhm, H.; Chueh, W.C. Redox activity of surface oxygen anions in oxygen-deficient perovskite oxides during electrochemical reactions. *Nat. Commun.* **2015**, *6*, 6097. [CrossRef] [PubMed]
16. Saubanère, M.; McCalla, E.; Tarascon, J.M.; Doublet, M.L. The intriguing question of anionic redox in high-energy density cathodes for Li-ion batteries. *Energy Environ. Sci.* **2016**, *9*, 984–991. [CrossRef]
17. Xie, Y.; Saubanère, M.; Doublet, M.L. Requirements for reversible extra-capacity in Li-rich layered oxides for Li-ion batteries. *Energy Environ. Sci.* **2017**, *10*, 266–274. [CrossRef]
18. Yabuuchi, N.; Nakayama, M.; Takeuchi, M.; Komaba, S.; Hashimoto, Y.; Mukai, T.; Shiiba, H.; Sato, K.; Kobayashi, Y.; Nakao, A.; et al. Origin of stabilization and destabilization in solid-state redox reaction of oxide ions for lithium-ion batteries. *Nat. Commun.* **2016**, *7*, 13814. [CrossRef] [PubMed]
19. Pearce, P.E.; Perez, A.J.; Rousse, G.; Saubanère, M.; Batuk, D.; Foix, D.; McCalla, E.; Abakumov, A.M.; Van Tendeloo, G.; Doublet, M.-L.; et al. Evidence for anionic redox activity in a tridimensional-ordered Li-rich positive electrode β-Li_2IrO_3. *Nat. Mater.* **2017**, *16*, 580–586. [CrossRef] [PubMed]
20. McCalla, E.; Abakumov, A.M.; Saubanere, M.; Foix, D.; Berg, E.J.; Rousse, G.; Doublet, M.L.; Gonbeau, D.; Novak, P.; Van Tendeloo, G.; et al. Visualization of O–O peroxo-like dimers in high-capacity layered oxides for Li-ion batteries. *Science* **2015**, *350*, 1516–1521. [CrossRef] [PubMed]
21. Luo, K.; Roberts, M.R.; Hao, R.; Guerrini, N.; Pickup, D.M.; Liu, Y.-S.; Edström, K.; Guo, J.; Chadwick, A.V.; Duda, L.C.; et al. Charge-compensation in 3d-transition-metal-oxide intercalation cathodes through the generation of localized electron holes on oxygen. *Nat. Chem.* **2016**, *8*, 684–691. [CrossRef] [PubMed]
22. Seo, D.-H.; Lee, J.; Urban, A.; Malik, R.; Kang, S.; Ceder, G. The structural and chemical origin of the oxygen redox activity in layered and cation-disordered Li-excess cathode materials. *Nat. Chem.* **2016**, *8*, 692–697. [CrossRef] [PubMed]
23. Grimaud, A.; Demortiere, A.; Saubanere, M.; Dachraoui, W.; Duchamp, M.; Doublet, M.-l.; Tarascon, J.-M. Activation of surface oxygen sites on an iridium-based model catalyst for the oxygen evolution reaction. *Nat. Energy* **2016**, *2*, 16189. [CrossRef]
24. Torrance, J.B.; Metzger, R.M. Role of the Madelung energy in hole conductivity in copper oxides: Difference between semiconductors and high-Tc superconductors. *Phys. Rev. Lett.* **1989**, *63*, 1515–1518. [CrossRef] [PubMed]
25. Chen, H.; Umezawa, N. Hole localization, migration, and the formation of peroxide anion in perovskite $SrTiO_3$. *Phys. Rev. B* **2014**, *90*, 035202. [CrossRef]
26. Herlihy, D.M.; Waegele, M.M.; Chen, X.; Pemmaraju, C.D.; Prendergast, D.; Cuk, T. Detecting the oxyl radical of photocatalytic water oxidation at an n-$SrTiO_3$/aqueous interface through its subsurface vibration. *Nat. Chem.* **2016**, *8*, 549–555. [CrossRef] [PubMed]
27. Chen, X.; Choing, S.N.; Aschaffenburg, D.J.; Pemmaraju, C.D.; Prendergast, D.; Cuk, T. The Formation Time of Ti–O(·) and Ti–O(·)-Ti Radicals at the n-$SrTiO_3$/Aqueous Interface during Photocatalytic Water Oxidation. *J. Am. Chem. Soc.* **2017**, *139*, 1830–1841. [CrossRef] [PubMed]

28. Campet, G.; Portier, J.; Subramanian, M.A. Electronegativity versus Fermi energy in oxides: The role of formal oxidation state. *Mater. Lett.* **2004**, *58*, 437–438. [CrossRef]
29. Matar, S.F.; Campet, G.; Subramanian, M.A. Electronic properties of oxides: Chemical and theoretical approaches. *Prog. Solid State Chem.* **2011**, *39*, 70–95. [CrossRef]
30. Mortier, W.J.; Gosh, S.K.; Shankar, S. Electronegativity Equalization Method for the Calculation of Atomic Charges in Molecules. *J. Am. Chem. Soc.* **1986**, *108*, 4315–4320. [CrossRef]
31. Van Genechten, K.A.; Mortier, W.J.; Geerlings, P. Intrinsic framework electronegativity: A novel concept in solid state chemistry. *J. Chem. Phys.* **1987**, *86*, 5063–5071. [CrossRef]
32. Saubanère, M.; Ben Yahia, M.; Lebègue, S.; Doublet, M.-L. An intuitive and efficient method for cell voltage prediction of lithium and sodium-ion batteries. *Nat. Commun.* **2014**, *5*, 5559. [CrossRef] [PubMed]
33. Zaanen, J.; Sawatzky, G.; Allen, J. Band gaps and electronic structure of transition-metal compounds. *Phys. Rev. Lett.* **1985**, *55*, 418–421. [CrossRef] [PubMed]
34. Saitoh, T.; Bocquet, A.E.; Mizokawa, T.; Fujimori, A. Systematic variation of the electronic structure of 3d transition-metal compounds. *Phys. Rev. B* **1995**, *52*, 7934–7938. [CrossRef]
35. Hong, W.T.; Stoerzinger, K.A.; Moritz, B.; Devereaux, T.P.; Yang, W.; Shao-Horn, Y. Probing $LaMO_3$ Metal and Oxygen Partial Density of States Using X-ray Emission, Absorption, and Photoelectron Spectroscopy. *J. Phys. Chem. C* **2015**, *119*, 2063–2072. [CrossRef]
36. Bocquet, A.E.; Mizokawa, T.; Saitoh, T.; Namatame, H.; Fujimori, A. Electronic structure of 3*d*-transition-metal compounds by analysis of the 2*p* core-level photoemission spectra. *Phys. Rev. B Condens. Matter* **1992**, *46*, 3771–3784. [CrossRef] [PubMed]
37. Suntivich, J.; Hong, W.T.; Lee, Y.-L.; Rondinelli, J.M.; Yang, W.; Goodenough, J.B.; Dabrowski, B.; Freeland, J.W.; Shao-horn, Y. Estimating Hybridization of Transition Metal and Oxygen States in Perovskites from O K-edge X-ray Absorption Spectroscopy. *J. Phys. Chem. C* **2014**, *118*, 1856–1863. [CrossRef]
38. Bocquet, A.E.; Fujimori, A.; Mizokawa, T.; Saitoh, T.; Namatame, H.; Suga, S.; Kimizuka, N.; Takeda, Y.; Takano, M. Electronic structure of $SrFe^{4+}O_3$ and related Fe perovskite oxides. *Phys. Rev. B* **1992**, *45*, 1561–1570. [CrossRef]
39. Potze, R.; Sawatzky, G.; Abbate, M. Possibility for an intermediate-spin ground state in the charge-transfer material $SrCoO_3$. *Phys. Rev. B Condens. Matter* **1995**, *51*, 11501–11506. [CrossRef] [PubMed]
40. Abbate, M.; Zampieri, G.; Okamoto, J.; Fujimori, A.; Kawasaki, S.; Takano, M. X-ray absorption of the negative charge-transfer material $SrFe_{1-x}Co_xO_3$. *Phys. Rev. B* **2002**, *65*. [CrossRef]
41. Bisogni, V.; Catalano, S.; Green, R.J.; Gibert, M.; Scherwitzl, R.; Huang, Y.; Strocov, V.N.; Zubko, P.; Balandeh, S.; Triscone, J.-M.; et al. Ground-state oxygen holes and the metal–insulator transition in the negative charge-transfer rare-earth nickelates. *Nat. Commun.* **2016**, *7*, 13017. [CrossRef] [PubMed]
42. Grisolia, M.N.; Varignon, J.; Sanchez-Santolino, G.; Arora, A.; Valencia, S.; Varela, M.; Abrudan, R.; Weschke, E.; Schierle, E.; Rault, J.E.; et al. Hybridization-controlled charge transfer and induced magnetism at correlated oxide interfaces. *Nat. Phys.* **2016**, *12*, 484–492. [CrossRef] [PubMed]
43. Mizumaki, M.; Fujii, H.; Yoshii, K.; Hayashi, N.; Saito, T.; Shimakawa, Y.; Uozumi, T.; Takano, M. Electronic structure of $BaFeO_3$ studied by X-ray spectroscopy. *Phys. Status Solidi* **2015**, *12*, 818–821. [CrossRef]
44. Mizumaki, M.; Saito, T.; Uozumi, T.; Shimakawa, Y. X-ray Spectroscopic Studies of A-Site Ordered Perovskite $LaMn_3B_4O_{12}$ (B = V, Cr). *e-J. Surf. Sci. Nanotechnol.* **2012**, *10*, 575–577. [CrossRef]
45. Lankhorst, M.H.R.; Bouwmeester, H.J.M.; Verweij, H. Use of the rigid band formalism to interpret the relationship between O chemical potential and electron concentration in $La_{1-x}Sr_xCoO_{3-\delta}$. *Phys. Rev. Lett.* **1996**, *77*, 2989–2992. [CrossRef] [PubMed]
46. Merkle, R.; Mastrikov, Y.A.; Kotomin, E.A.; Kuklja, M.M.; Maier, J. First Principles Calculations of Oxygen Vacancy Formation and Migration in $Ba_{1-x}Sr_xCo_{1-y}Fe_yO_{3-\delta}$ Perovskites. *J. Electrochem. Soc.* **2012**, *159*, B219. [CrossRef]
47. Mastrikov, Y.A.; Merkle, R.; Heifets, E.; Kotomin, E.A.; Maier, J. Pathways for Oxygen Incorporation in Mixed Conducting Perovskites: A DFT-Based Mechanistic Analysis for (La, Sr)$MnO_{3-\delta}$. *J. Phys. Chem. C* **2010**, *114*, 3017–3027. [CrossRef]
48. Lee, Y.S.; Lee, J.S.; Noh, T.W.; Byun, D.Y.; Yoo, K.S.; Yamaura, K.; Takayama-Muromachi, E. Systematic trends in the electronic structure parameters of the 4*d* transition-metal oxides $SrMO_3$ (M = Zr, Mo, Ru, and Rh). *Phys. Rev. B* **2003**, *67*. [CrossRef]

49. Sathiya, M.; Rousse, G.; Ramesha, K.; Laisa, C.P.; Vezin, H.; Sougrati, M.T.; Doublet, M.-L.; Foix, D.; Gonbeau, D.; Walker, W.; et al. Reversible anionic redox chemistry in high-capacity layered-oxide electrodes. *Nat. Mater.* **2013**, *12*, 827–835. [CrossRef] [PubMed]
50. Yabuuchi, N.; Takeuchi, M.; Nakayama, M.; Shiiba, H.; Ogawa, M.; Nakayama, K.; Ohta, T.; Endo, D.; Ozaki, T.; Inamasu, T.; et al. High-capacity electrode materials for rechargeable lithium batteries: Li_3NbO_4-based system with cation-disordered rocksalt structure. *Proc. Natl. Acad. Sci. USA* **2015**, *112*, 7650–7655. [CrossRef] [PubMed]
51. Thackeray, M.M.; Kang, S.-H.; Johnson, C.S.; Vaughey, J.T.; Benedek, R.; Hackney, S.A. Li_2MnO_3-stabilized $LiMO_2$ (M = Mn, Ni, Co) electrodes for lithium-ion batteries. *J. Mater. Chem.* **2007**, *17*, 3112. [CrossRef]
52. Lu, Z.; Beaulieu, L.Y.; Donaberger, R.A.; Thomas, C.L.; Dahn, J.R. Synthesis, Structure, and Electrochemical Behavior of $Li[Ni_xLi_{1/3-2x/3}Mn_{2/3-x/3}]O_2$. *J. Electrochem. Soc.* **2002**, *149*, A778. [CrossRef]
53. Grimaud, A.; Carlton, C.E.; Risch, M.; Hong, W.T.; May, K.J.; Shao-horn, Y. Oxygen Evolution Activity and Stability of $Ba_6Mn_5O_{16}$, $Sr_4Mn_2CoO_9$, and $Sr_6Co_5O_{15}$: The Influence of Transition Metal Coordination. *J. Phys. Chem. C* **2013**, *117*, 25926–25932. [CrossRef]
54. Villesuzanne, A.; Whangbo, M.-H. Comparative electronic band structure study of the intrachain ferromagnetic versus antiferromagnetic coupling in the magnetic oxides $Ca_3Co_2O_6$ and Ca_3FeRhO_6. *Inorg. Chem.* **2005**, *44*, 6339–6345. [CrossRef] [PubMed]
55. Torrance, J.B.; Lacorre, P.; Nazzal, A.I.; Ansaldo, E.J.; Niedermayer, C. Systematic study of insulator-metal transitions in perovskites $RNiO_3$. *Phys. Rev. B Condens. Matter* **1992**, *45*, 8209–8212. [CrossRef] [PubMed]
56. Shannon, R.D. Revised Effective Ionic Radii and Systematic Studies of Interatomie Distances in Halides and Chaleogenides. *Acta Cryst.* **1976**, *A32*, 751. [CrossRef]
57. Nemudry, A.; Goldberg, E.L.; Aguirre, M.; Alario-Franco, M.A. Electrochemical topotactic oxidation of nonstoichiometric perovskites at ambient temperature. *Solid State Sci.* **2002**, *4*, 677–690. [CrossRef]
58. Grenier, J.C.; Wattiaux, A.; Doumerc, J.P.; Dordor, P.; Fournes, L.; Chaminade, J.P.; Pouchard, M. Electrochemical Oxygen Intercalation into Oxide Networks. *J. Solid State Chem.* **1992**, *96*, 20–30. [CrossRef]
59. Götzfried, T.; Reller, A.; Ebbinghaus, S.G. Structural and Magnetic Properties of Hexagonal Perovskites $La_{1.2}Sr_{2.7}MO_{7.33}$ (M = Ru, Ir) Containing Peroxide Ions. *Inorg. Chem.* **2005**, *44*, 6550–6557. [CrossRef] [PubMed]
60. Grasset, F.; Dussarrat, C.; Darriet, J.; Schweitzer, A.A. Preparation, thermal stability and crystal structure of a new ruthenium(V) oxide containing peroxide ions: $Ba_2Ru_5O_9(O_2)$. Structural relationships to the hexagonal-type perovskite. *J. Mater. Chem.* **1997**, *7*, 1911–1915. [CrossRef]
61. Doornkamp, C.; Ponec, V. The universal character of the Mars and Van Krevelen mechanism. *J. Mol. Catal. A Chem.* **2000**, *162*, 19–32. [CrossRef]
62. Mars, P.; van Krevelen, D.W. Oxidations carried out by means of vanadium oxide catalysts. *Chem. Eng. Sci.* **1954**, *3*, 41–59. [CrossRef]
63. Grimaud, A.; Hong, W.T.; Shao-Horn, Y.; Tarascon, J.M. Anionic redox processes for electrochemical devices. *Nat. Mater.* **2016**, *15*, 121–126. [CrossRef] [PubMed]
64. Bielanski, A.; Haber, J. Oxygen in Catalysis on Transition Metal Oxides. *Catal. Rev.* **1979**, *19*, 1–41. [CrossRef]
65. Croué, K.; Jolivet, J.-P.; Larcher, D. Direct Determination of Oxide Surface Free Energy through Potentiometric Measurements. *Electrochem. Solid-State Lett.* **2012**, *15*, F8. [CrossRef]
66. Grimaud, A.; May, K.J.; Carlton, C.E.; Lee, Y.L.; Risch, M.; Hong, W.T.; Zhou, J.; Shao-Horn, Y. Double perovskites as a family of highly active catalysts for oxygen evolution in alkaline solution. *Nat. Commun.* **2013**, *4*, 2439. [CrossRef] [PubMed]
67. Bockris, J.O.M.; Otagawa, T. The electrocatalysis of oxygen evolution on perovskites. *J. Electrochem. Soc.* **1984**, *131*, 290–302. [CrossRef]
68. Bockris, J.O.; Otagawa, T. Mechanism of oxygen evolution on perovskites. *J. Phys. Chem.* **1983**, *87*, 2960–2971. [CrossRef]
69. Dowden, D.A. Crystal and Ligand Field Models of Solid Catalysts. *Catal. Rev.* **1972**, *5*, 1–32. [CrossRef]
70. Calle-Vallejo, F.; Inoglu, N.G.; Su, H.-Y.; Martínez, J.I.; Man, I.C.; Koper, M.T.M.; Kitchin, J.R.; Rossmeisl, J. Number of outer electrons as descriptor for adsorption processes on transition metals and their oxides. *Chem. Sci.* **2013**, *4*, 1245. [CrossRef]

71. Suntivich, J.; Gasteiger, H.A.; Yabuuchi, N.; Nakanishi, H.; Goodenough, J.B.; Shao-Horn, Y. Design principles for oxygen-reduction activity on perovskite oxide catalysts for fuel cells and metal–air batteries. *Nat. Chem.* **2011**, *3*, 546–550. [CrossRef] [PubMed]
72. Suntivich, J.; May, K.J.; Gasteiger, H.A.; Goodenough, J.B.; Shao-Horn, Y. A Perovskite Oxide Optimized for Oxygen Evolution Catalysis from Molecular Orbital Principles. *Science* **2011**, *334*, 1383–1385. [CrossRef] [PubMed]
73. Meadowcroft, D.B. Low-cost Oxygen Electrode Material. *Nature* **1970**, *226*, 847–848. [CrossRef] [PubMed]
74. Matsumoto, Y.; Sato, E. Electrocatalytic properties of transition metal oxides for oxygen evolution reaction. *Mater. Chem. Phys.* **1986**, *14*, 397–426. [CrossRef]
75. Han, B.; Stoerzinger, K.A.; Tileli, V.; Gamalski, A.D.; Stach, E.A.; Shao-Horn, Y. Nanoscale structural oscillations in perovskite oxides induced by oxygen evolution. *Nat. Mater.* **2016**, *16*, 121–126. [CrossRef] [PubMed]
76. Raabe, S.; Mierwaldt, D.; Ciston, J.; Uijttewaal, M.; Stein, H.; Hoffmann, J.; Zhu, Y.; Blöchl, P.; Jooss, C. In Situ Electrochemical Electron Microscopy Study of Oxygen Evolution Activity of Doped Manganite Perovskites. *Adv. Funct. Mater.* **2012**, *22*, 3378–3388. [CrossRef]
77. Risch, M.; Grimaud, A.; May, K.J.; Stoerzinger, K.A.; Chen, T.J.; Mansour, A.N.; Shao-Horn, Y. Structural Changes of Cobalt-Based Perovskites upon Water Oxidation Investigated by EXAFS. *J. Phys. Chem. C* **2013**, *117*, 8628–8635. [CrossRef]
78. Man, I.C.; Su, H.-Y.; Calle-Vallejo, F.; Hansen, H.A.; Martínez, J.I.; Inoglu, N.G.; Kitchin, J.; Jaramillo, T.F.; Nørskov, J.K.; Rossmeisl, J. Universality in Oxygen Evolution Electrocatalysis on Oxide Surfaces. *ChemCatChem* **2011**, *3*, 1159–1165. [CrossRef]
79. Nørskov, J.K.; Rossmeisl, J.; Logadottir, A.; Lindqvist, L.; Kitchin, J.R.; Bligaard, T.; Jónsson, H. Origin of the Overpotential for Oxygen Reduction at a Fuel-Cell Cathode. *J. Phys. Chem. B* **2004**, *108*, 17886–17892. [CrossRef]
80. Petrie, J.R.; Cooper, V.R.; Freeland, J.W.; Meyer, T.L.; Zhang, Z.; Lutterman, D.A.; Lee, H.N. Enhanced Bifunctional Oxygen Catalysis in Strained $LaNiO_3$ Perovskites. *J. Am. Chem. Soc.* **2016**, *138*, 2488–2491. [CrossRef] [PubMed]
81. Mavros, M.G.; Tsuchimochi, T.; Kowalczyk, T.; McIsaac, A.; Wang, L.-P.; Voorhis, T.V. What Can Density Functional Theory Tell Us about Artificial Catalytic Water Splitting? *Inorg. Chem.* **2014**, *53*, 6386–6397. [CrossRef] [PubMed]
82. Betley, T.A.; Wu, Q.; Van Voorhis, T.; Nocera, D.G. Electronic Design Criteria for O−O Bond Formation via Metal−Oxo Complexes. *Inorg. Chem.* **2008**, *47*, 1849–1861. [CrossRef] [PubMed]
83. Vasala, S.; Karppinen, M. $A_2B'B''O_6$ perovskites: A review. *Prog. Solid State Chem.* **2015**, *43*, 1–36. [CrossRef]
84. Diaz-Morales, O.; Raaijman, S.; Kortlever, R.; Kooyman, P.J.; Wezendonk, T.; Gascon, J.; Fu, W.T.; Koper, M.T.M. Iridium-based double perovskites for efficient water oxidation in acid media. *Nat. Commun.* **2016**, *7*, 12363. [CrossRef] [PubMed]
85. Seitz, L.C.; Dickens, C.F.; Nishio, K.; Hikita, Y.; Montoya, J.; Doyle, A.; Kirk, C.; Vojvodic, A.; Hwang, H.Y.; Norskov, J.K.; et al. A highly active and stable $IrO_x/SrIrO_3$ catalyst for the oxygen evolution reaction. *Science* **2016**, *353*, 1011–1014. [CrossRef] [PubMed]
86. Chang, S.H.; Danilovic, N.; Chang, K.-C.; Subbaraman, R.; Paulikas, A.P.; Fong, D.D.; Highland, M.J.; Baldo, P.M.; Stamenkovic, V.R.; Freeland, J.W.; et al. Functional links between stability and reactivity of strontium ruthenate single crystals during oxygen evolution. *Nat. Commun.* **2014**, *5*, 4191. [CrossRef] [PubMed]
87. Binninger, T.; Mohamed, R.; Waltar, K.; Fabbri, E.; Levecque, P.; Kötz, R.; Schmidt, T.J. Thermodynamic explanation of the universal correlation between oxygen evolution activity and corrosion of oxide catalysts. *Sci. Rep.* **2015**, *5*, 12167. [CrossRef] [PubMed]
88. Björneholm, O.; Hansen, M.H.; Hodgson, A.; Liu, L.-M.; Limmer, D.T.; Michaelides, A.; Pedevilla, P.; Rossmeisl, J.; Shen, H.; Tocci, G.; et al. Water at Interfaces. *Chem. Rev.* **2016**, *116*, 7698–7726. [CrossRef] [PubMed]
89. Rong, X.; Kolpak, A.M. Ab Initio Approach for Prediction of Oxide Surface Structure, Stoichiometry, and Electrocatalytic Activity in Aqueous Solution. *J. Phys. Chem. Lett.* **2015**, *6*, 1785–1789. [CrossRef] [PubMed]
90. Tascón, J.M.D.; González Tejuca, L. Catalytic activity of perovskite-type oxides $LaMeO_3$. *React. Kinet. Catal. Lett.* **1980**, *15*, 185–191. [CrossRef]

91. Demazeau, G.; Oh-Kim, E.O.; Choy, J.-H.; Hagenmuller, P. La stabilisation partielle du manganese(V) en coordinence octahedrique au sein d'un reseau oxygéné: Préparation et caractérisation physico-chimique du composé La_2LiMnO_{6-x}. *J. Solid* **1992**, *101*, 221–228.
92. Demazeau, G.; Buffat, B.; Pouchard, M.; Hagenmuller, P. Recent developments in the field of high oxidation states of transition elements in oxides stabilization of Six-coordinated Iron(V). *Z. Anorg. Allg. Chem.* **1982**, *491*, 60–66. [CrossRef]
93. Buffat, B.; Tljilier, M.H.; Dexpert, H.; Demazeau, G. X-ray absorption investigation of some high oxidation states of six-co-ordinated iron in oxides of perovskite or k_2nif_4 -type structures. *J. Phys. Chem. Solids* **1986**, *47*, 491–496. [CrossRef]
94. Yagi, S.; Yamada, I.; Tsukasaki, H.; Seno, A.; Murakami, M.; Fujii, H.; Chen, H.; Umezawa, N.; Abe, H.; Nishiyama, N.; et al. Covalency-reinforced oxygen evolution reaction catalyst. *Nat. Commun.* **2015**, *6*, 8249. [CrossRef] [PubMed]
95. Cheng, X.; Fabbri, E.; Nachtegaal, M.; Castelli, I.E.; El Kazzi, M.; Haumont, R.; Marzari, N.; Schmidt, T.J. Oxygen Evolution Reaction on $La_{1-x}Sr_xCoO_3$ Perovskites: A Combined Experimental and Theoretical Study of Their Structural, Electronic, and Electrochemical Properties. *Chem. Mater.* **2015**, *27*, 7662–7672. [CrossRef]
96. May, K.J.; Carlton, C.E.; Stoerzinger, K.A.; Risch, M.; Suntivich, J.; Lee, Y.-L.; Grimaud, A.; Shao-Horn, Y. Influence of oxygen evolution during water oxidation on the surface of perovskite oxide catalysts. *J. Phys. Chem. Lett.* **2012**, *3*, 3264–3270. [CrossRef]
97. Tahini, H.A.; Tan, X.; Schwingenschlögl, U.; Smith, S.C. In Operando Self-Healing of Perovskite Electrocatalysts: A Case Study of $SrCoO_3$ for the Oxygen Evolution Reaction. *Part. Part. Syst. Charact.* **2017**, *34*, 1600280. [CrossRef]
98. Tarancón, A.; Burriel, M.; Santiso, J.; Skinner, S.J.; Kilner, J.A. Advances in layered oxide cathodes for intermediate temperature solid oxide fuel cells. *J. Mater. Chem.* **2010**, *20*, 3799. [CrossRef]
99. Voorhoeve, R.J.H.; Johnson, D.W.; Remeika, J.P.; Gallagher, P.K. Perovskite Oxides: Materials Science in Catalysis. *Science* **1977**, *195*, 827–833. [CrossRef] [PubMed]
100. Voorhoeve, R.J.H.; Remeika, J.P.; Trimble, L.E. Defect Chemistry and Catalysis in Oxidation and Reduction over Perovskite-type Oxides. *Ann. N. Y. Acad. Sci.* **1976**, *272*, 3–21. [CrossRef]
101. Yamazoe, N.; Teraoka, Y. Oxidation Catalysis of Perovskites—Relationships to Bulk Structure and Composition (Valency, Defects, etc.). *Catal. Today* **1990**, *8*, 175–199. [CrossRef]
102. Yamazoe, N.; Teraoka, Y.; Seiyama, T. TPD and XPS Thermal Behavior of Adsorbed Oxygen in $La_{1-x}Sr_xCoO_3$. *Chem. Lett.* **1981**, *10*, 1767–1770. [CrossRef]
103. Panov, G.; Dubkov, K.; Starokon, E. Active oxygen in selective oxidation catalysis. *Catal. Today* **2006**, *117*, 148–155. [CrossRef]
104. Meng, Q.; Wang, W.; Weng, X.; Liu, Y.; Wang, H.; Wu, Z. Active Oxygen Species in $La_{n+1}Ni_nO_{3n+1}$ Layered Perovskites for Catalytic Oxidation of Toluene and Methane. *J. Phys. Chem. C* **2016**, *120*, 3259–3266. [CrossRef]
105. Pereñíguez, R.; Hueso, J.L.; Gaillard, F.; Holgado, J.P.; Caballero, A. Study of Oxygen Reactivity in $La_{1-x}Sr_xCoO_{3-\delta}$ Perovskites for Total Oxidation of Toluene. *Catal. Lett.* **2012**, *142*, 408–416. [CrossRef]
106. Tejuca, L.G.; Fierro, J.L.G.; Tascon, J.M.D. Structure and Reactivity of Perovskite-Type Oxides. *Adv. Catal.* **1989**, *36*, 237–328.
107. Rremenic, G.; Nieto, J.M.L.; Tascon, J.M.D.; Tejuca, L.G. Chemisorption and Catalysis on $LaMO_3$ Oxides. *J. Chem. Soc. Faraday Trans.* **1985**, *1*, 939–949. [CrossRef]
108. Gellings, P.J.; Bouwmeester, H.J.M. Solid state aspects of oxidation catalysis. *Catal. Today* **2000**, *58*, 1–53. [CrossRef]
109. Mildner, S.; Beleggia, M.; Mierwaldt, D.; Hansen, T.W.; Wagner, J.B.; Yazdi, S.; Kasama, T.; Ciston, J.; Zhu, Y.; Jooss, C. Environmental TEM Study of Electron Beam Induced Electrochemistry of $Pr_{0.64}Ca_{0.36}MnO_3$ Catalysts for Oxygen Evolution. *J. Phys. Chem. C* **2015**, *119*, 5301–5310. [CrossRef]
110. Halat, D.M.; Dervişoğlu, R.; Kim, G.; Dunstan, M.T.; Blanc, F.; Middlemiss, D.S.; Grey, C.P. Probing Oxide-Ion Mobility in the Mixed Ionic-Electronic Conductor $La_2NiO_{4+\delta}$ by Solid-State $^{(17)}$O MAS NMR Spectroscopy. *J. Am. Chem. Soc.* **2016**, *138*, 11958–11969. [CrossRef] [PubMed]
111. Wohlfahrt-Mehrens, M.; Heitbaum, J. Oxygen evolution on Ru and RuO_2 electrodes studied using isotope labelling and on-line mass spectrometry. *J. Electroanal. Chem. Interfacial Electrochem.* **1987**, *237*, 251–260. [CrossRef]

112. Fierro, S.; Nagel, T.; Baltruschat, H.; Comninellis, C. Investigation of the oxygen evolution reaction on Ti/IrO_2 electrodes using isotope labelling and on-line mass spectrometry. *Electrochem. Commun.* **2007**, *9*, 1969–1974. [CrossRef]
113. Diaz-Morales, O.; Calle-Vallejo, F.; de Munck, C.; Koper, M.T.M. Electrochemical water splitting by gold: Evidence for an oxide decomposition mechanism. *Chem. Sci.* **2013**, *4*, 2334. [CrossRef]